Establishing the content in trace and minor elements of magnetite as a biosignature of magnetotactic bacteria

François Mathon, Matthieu Amor, François Guyot, Nicolas Menguy, Christopher Lefevre, Vincent Busigny

Establishing the content in trace and minor elements of magnetite as a biosignature of magnetotactic bacteria

François P. Mathon[1,2], Matthieu Amor[3], François Guyot[4], Nicolas Menguy[4], Christopher T. Lefevre[2], Vincent Busigny[1,*]

[1] Université de Paris, Institut de Physique du Globe de Paris, CNRS, F-75005, Paris, France

[2] Aix-Marseille Université, CEA, CNRS, BIAM, 13115 Saint-Paul-lez-Durance, France

[3] Univ. Lyon, ENSL, UCBL, UJM, CNRS, LGL-TPE, F-69007 Lyon, France

[4] Muséum National d'Histoire Naturelle, Sorbonne Université, UMR CNRS 7590. Institut de Minéralogie, de Physique des Matériaux et de Cosmochimie (IMPMC), Paris, France

*For correspondence, e-mail to: busigny@ipgp.fr

ABSTRACT

Magnetotactic bacteria (MTB) produce intracellular magnetite (Fe_3O_4) nanoparticles in a genetically controlled manner. They may represent some of the oldest biomineralizing organisms available in the geological record, but identification of their fossils remains highly debated. While organic molecules are degraded during diagenesis and metamorphic processes, MTB magnetite nanocrystals can be efficiently preserved in the rock record and are referred to as magnetofossils. Experimental work on the freshwater bacterium *Magnetospirillum magneticum* strain AMB-1 has demonstrated specific minor and trace element patterns distinct from those of abiotic magnetite, and were proposed as a tool for magnetofossil identification. These promising geochemical signatures need to be validated in diverse MTB strains to be used for paleontological reconstruction. Here, we cultivated a marine MTB (*Magnetovibrio blakemorei* strain MV-1) under various chemical conditions to test possible generalization of this new proxy. MV-1 was grown under various Fe concentrations (50, 100 and 150 μM) and redox states using either Fe(II)-ascorbate or Fe(III)-citrate as Fe sources. The chemical compositions of the growth media and extracted magnetite crystals were determined by ICP-MS analyses to quantify the partitioning of trace and minor elements between magnetite and solution. Results show that partition coefficients do not depend at first order on the Fe concentration and redox state, a crucial conclusion for potential application to natural systems. A comparison of the two strains shows that MV-1 magnetite generally contains higher concentrations of impurities than AMB-1 magnetite. However, a number of elements possess similar partition coefficients and may represent useful chemical proxies for testing the biological origin of magnetite. These consistent elements can be separated into three groups. The first group is composed of elements (Co, Mn, Pb, Sr) highly depleted in MTB magnetite relative to abiotic magnetite. The second group contains elements with similar partitioning in MTB and abiotic magnetite, including Ca and Li. This group may serve as a reference for constraining a paleo-fluid composition. The last group contains elements (Mo, Sn, Se) enriched in MTB magnetite relative to abiotic magnetite. Such enrichments might be related to biological function of those elements. Chemical patterns determined from laboratory experiments therefore represent promising chemical proxies to identify MTB magnetite in the rock record but now need to be tested in modern natural environments, where MTB and surrounding solution can be jointly collected.

Keywords: *magnetotactic bacteria; biomineralization; magnetite; biosignature*

1. Introduction

Magnetotactic bacteria (MTB) are ubiquitous microorganisms found in most aquatic environments near oxic-anoxic transition zones (OATZ). They produce ferrimagnetic nanocrystals of magnetite (Fe_3O_4) or greigite (Fe_3S_4) in organelles called magnetosomes, which consist of a bi-layered lipid membrane surrounding a single magnetite or greigite nanoparticle (Bazylinski and Frankel, 2004; Faivre and Schüler, 2008). Magnetosome formation is genetically controlled, and requires about ~30 genes clustered in a specific region of the genome (Murat et al., 2010). In most MTB, magnetic particles are organized in chains, which provide the cell with a permanent magnetic dipole and enable it to align along the geomagnetic field lines and swim efficiently towards OATZ. MTB show a great diversity in terms of morphology, physiology, and crystal habits (Lefèvre and Bazylinski, 2013; Liu et al., 2021a, 2021b). Several studies based on phylogenetic analyses proposed that MTB emerged between 2.5 to 3.2 Ga (Lefèvre and Wu, 2013; Lefèvre et al., 2013; Lin et al., 2017; Goswami et al., 2022). This possibility has been linked to environmental conditions of the Archean Earth and more specifically to the presence of redox gradients in "oxygen oases" of a globally anoxic ocean that may have represented ideal habitats for the emergence of MTB (Lin et al., 2017). Upon bacterial death, MTB magnetite can be trapped in sediments and efficiently preserved in sedimentary rocks over geological times (see recent reviews in Amor et al, 2020; Goswami et al., 2022; and references therein). Identification of the fossil mineralogical remains of MTB (hereafter referred to as magnetofossils) in ancient rocks would thus provide strong constrains on the evolution of life and paleoenvironments over geological times.

Several studies attempted to pinpoint magnetofossils in the sedimentary record (Chang and Kirschvink, 1989; Akai et al., 1997; Kopp and Kirschvink, 2008). While organic remains of cellular bodies can hardly be identified in such ancient rocks, magnetite crystals are efficiently preserved. Magnetite is abundantly recorded in Archean sedimentary rocks such as banded iron formations (BIFs) from Australia, Africa, Brazil and North America (Klein, 2005), illustrating the high preservation capacity of magnetite. The oldest putative occurrences of magnetofossils were reported in stromatolithic limestones and cherts from the 2.0 Ga-old Gunflint Formation, Northern America (Chang and Kirschvink, 1989) and the 2.7 Ga-old Tumbiana Formation, Western Australia (Akai et al., 1997). These conclusions were reached based on the analysis of magnetite size and shape as well as the presence of magnetite chains in the case of Gunflint

sediments. Indeed, nanocrystals of magnetite produced by MTB usually show a narrow size distribution and specific morphologies (Devouard et al., 1998; Busek et al., 2001; Arato et al., 2005). These criteria can be used to support a biological origin but are not sufficient (Faivre et Zuddas, 2006). Thomas-Keprta et al. (2000) proposed the use of six criteria for magnetofossil identification, which were later completed by additional magnetic, chemical and isotopic indicators (see Amor et al., 2020 and references therein). While morphological and magnetic criteria have extensively been explored (see Thomas-Keprta et al., 2000 and references therein; Buseck et al., 2001; Egli, 2004; Heslop et al., 2014; Chang et al., 2016), chemical and isotopic signatures need further support from experimental evidences to be established as unambiguous proxies of MTB activity (Amor et al., 2015, 2016). In the present contribution, we focus on the elemental content of magnetite.

The trace and minor element content of magnetite synthesized by MTB was hypothesized to be lower than that of magnetite produced abiotically in aqueous solutions (Thomas-Keprta et al., 2000). In MTB, magnetite is synthesized in the magnetosome vesicle, which has a controlled chemical composition and is physically separated from the external solution (Faivre and Schüler, 2008; Amor et al., 2022). The presence of cation transporters in the magnetosome membrane and particularly Fe-specific transporters (Schuler, 2006; Uebe and Schüler, 2016) facilitates Fe accumulation into magnetosomes and excludes other metal ions, which in turn minimizes their incorporation into magnetite. The formation of magnetite precursors such as amorphous ferrihydrite (Frankel et al., 1983), phosphate-rich ferric hydroxide (Baumgartner et al., 2013) or hematite (Zhu et al., 2016; Le Nagard et al., 2019) may also play a role in trace element incorporation. Laboratory cultures of the magnetotactic bacterium *Magnetospirillum magneticum* strain AMB-1 quantified the degree of purity of biomagnetite (Amor et al., 2015). In this initial work, incorporation of most tested elements were at least 100-times lower in AMB-1 magnetite relative to its abiotic counterpart synthesized in the presence of the same trace and minor elements (Amor et al., 2015). Three exceptions were observed for Mo, Sn and Se that were preferentially incorporated into AMB-1 magnetite. Incorporation of trace elements into abiotic magnetite was shown to be controlled by ion size and valence following the lattice strain theory, as well as the energy levels of unfilled 3d orbitals for elements of the first series of transition metals (Cr to Zn) according to crystal field effects (Amor et al., 2023). Contrastingly, trace element incorporation into two MTB strains (AMB-1 and MSR-1) were compatible with a biopurification process excluding cations distinct from iron. These results demonstrate the biological origin of elemental patterns in magnetite, and represent a promising

tool for the identification of magnetofossils. Still, they need to be tested on additional magnetotactic strains to be firmly established as MTB signatures.

Here, we investigate the chemical composition of magnetite nanoparticles produced by *Magnetovibrio blakemorei* strain MV-1 following a similar approach to the previous work on AMB-1 and MSR-1 strains (Amor et al., 2015, 2023). Unlike the microaerophilic AMB-1 and MSR-1 strains isolated from freshwater (Matsunaga et al., 1991; Schüler and Köhler, 1992), MV-1 is a physiologically versatile marine bacterium that can grow under anoxic conditions using nitrous oxide (N_2O) as a terminal electron acceptor (Bazylinski et al., 2013). MV-1 also produces elongated prismatic magnetite, a crystal morphology distinct from the cuboctahedral magnetite produced by AMB-1 and MSR-1. MV-1 thus offers the opportunity to explore a third MTB strain living under different chemical conditions. Furthermore, we tested the sensitivity of MV-1 magnetite chemical composition to environmental parameters (i.e., iron concentration and redox state). The comparison of our results with the data previously obtained from distinct MTB strains and abiotic magnetite (Amor et al., 2015) enables us to establish robust chemical features of MTB magnetite useful for future identification of magnetofossils.

2. Materials and methods

2.1. MV-1 cultures

Magnetovibrio blakemorei strain MV-1 (DSMZ #18854) was cultivated under anoxic and reducing conditions in an artificial seawater mixed with a modified Wolfe's mineral solution (Wolin et al., 1963; Frankel et al., 1997). The growth medium (GM) was provided with either Fe(II)-ascorbate or Fe(III)-citrate at three different concentrations: 50, 100 and 150 µM. Iron sources were added to the GM from stock solutions prepared with $FeCl_2$ or $FeCl_3$ in HCl 0.05 M and mixed with either ascorbate or citrate solutions. Cultures were performed in 1-L Schott Duran® Pressure Plus flasks containing a growth medium solution as described in Bazylinski et al. (2013). Molecular oxygen (O_2) was replaced by nitrous oxide (N_2O), also used by bacteria as the terminal electron acceptor (Bazylinski et al., 2013). The redox indicator resazurin was added to the medium to detect any potential oxygen leak. The sources of organic carbon, also used as electron donor, were sodium succinate and sodium acetate, with concentrations in the initial growth medium of 2.4 and 0.8 g/L respectively. For all conditions, two replicates were obtained from 9 bottles of 1 L, in order to end up with enough bacteria for magnetosome separation, purification and analysis (Table 1). The cell density, estimated from the measurement of the optical density at 565 nm (OD_{565}), and the C_{mag} coefficient (Schüler et al.,

1995) were measured by spectrophotometry (Table S1). C_{mag} relies on the differential measurement of a culture's optical density when a magnet is oriented either vertically or horizontally close to the cell suspension. It is defined as the ratio of the maximum and minimum optical density and quantifies the capacity of bacteria to orientate along an external magnetic field. Iron concentration and redox state were monitored every 24 h during cultivation. They were determined using the ferrozine method as described in Viollier et al. (2000). Before starting the cultures, 10 mL of the initial GM were sampled to determine the initial iron concentration.

2.2. Cell lysis and purification of MV-1 magnetite

Initial cell density after inoculation was comprised between 2.3 and 6.6×10^8 cell/mL (day 0 in Table S1), determined from calibrated optical density (calibration preliminary obtained from cell counting using Malassez counting chamber after cultures of MV-1 with Fe concentrations ranging from 30 to 150 µM, n=24; Mathon, 2021). Cultures were stopped when cell density reached > 5.4×10^9 cell/mL and C_{mag} became roughly constant (Fig. S1), indicating that no additional magnetosomes were produced. Previous work demonstrated from C_{mag} and Fe uptake relationships that C_{mag} can be used as a proxy for magnetite formation (Schüler and Baeuerlein, 1998; see also Keshoju et al., 2007, for theoretical considerations about C_{mag}). Forty mL of the final growth medium were sub-sampled and filtered at 0.22 µm to measure the elemental concentrations of the residual GM solution. Magnetite nanoparticles were recovered following two steps: magnetosome extraction and magnetite purification. The first step was adapted from the protocols established by Ginet et al. (2011) and Mériaux et al. (2015). Cells were separated from the growth medium in Teflon flasks of 500 mL by centrifugation at 4500 rpm and 4°C during 45 min. The bacterial pellets were then pooled in a 50 mL polypropylene Falcon tube, centrifuged again at 4500 rpm and 4°C for 20 min. The final wet pellets weighed around 2 mg and were stored in a -20°C cold chamber. Then, MV-1 cells were suspended in a cold buffer (B1), containing HEPES (20 mM, pH = 7.5), NaCl (0.9 wt%), EDTA (1 mM), and glycerol (8 vol%) (Mériaux et al. 2015), together with a protease inhibitors cocktail (ref. P8849 Sigma-Aldrich; 20 µl of cocktail in 10 mL of B1), at 4°C to prevent samples from any degradation by enzymatic activity. The cells were lysed with a French Press operating at 7 MPa. Three lysis cycles were run successively (with no rinsing treatment between lysis cycles) to ensure complete disruption of the bacteria. Magnetosomes were magnetically recovered from the bacterial lysates by placing a magnet against the 50 mL Falcon tube containing the

magnetosome suspension. First, tubes were left for 1.5 h at 4°C before collecting the bacterial lysates. Magnetic recovery was repeated 4 times for 30 min in 40 mL of buffer (B1), and 5 times in 40 mL of a second buffer (B2) consisting of B1 buffer with no EDTA. Digestion of the magnetosome membrane was performed using a protocol adapted from Amor et al. (2015). Magnetosomes were sonicated at 100 Hz in 40 mL TES solution (0.5 vol%. Triton X, 10 mM EDTA, 1 vol% SDS) at 60°C for one hour. Then, they were washed twice with 40 mL Milli-Q water and recovered with a magnet. This operation was repeated 5 times before collecting and storing purified magnetite in Milli-Q water at -20°C.

2.3. Transmission electron microscopy characterization

Magnetite nanoparticles produced by MV-1 were observed by transmission electron microscopy (TEM) at each step of the purification process using a Tecnai G^2 BioTWIN (FEI Company) equipped with a CCD camera (Megaview III, Olympus Soft imaging Solutions GmbH) with an accelerating voltage of 100 kV or a JEOL JEM-2100F microscope operating at 200 kV. Magnetite size and shape were monitored inside the cells after recovery of whole bacteria, after magnetosome extraction from the bacterial lysates, and after digestion of the magnetosome membrane. All magnetite samples were initially deposited on 200-mesh copper grids coated with a formvar-carbon film. The grid was then washed three times with Milli-Q water (0.2 μm-filtered) to get rid of any trace of salts inherited from the GM or the buffer. The preparation of TEM grids was done at ambient air. Between twenty to thirty images were acquired for each type of sample (i.e. each experimental condition). Crystal lengths were measured on 600 to 1200 magnetite crystals (depending on samples) using the ImageJ software. Diffraction images were processed with the SingleCrystal software. We assessed the efficiency of magnetite nanoparticle collection by (i) calculating global mass balance on iron between initial and final states, and (ii) by constructing histograms showing the distribution of magnetite length (Mathon, 2021). We also estimated whether iron concentration impacted the magnetite size and if some nanocrystal populations were lost during the extraction and purification procedures (Fig. S2).

2.4. Trace and minor element analyses

Prior to mass spectrometry analyses, all samples were dissolved in Teflon beakers using ultrapure nitric acid (15 M HNO_3). Samples include purified magnetosomes extracted from bacterial pellets (< 1 mg) as well as filtered GM solution (10 mL). After evaporation, complete

digestion of organic components contained in the growth medium samples was ensured using hydrogen peroxide (H_2O_2) added to the nitric acid solution (100 µL of ultrapure H_2O_2 in 10 mL HNO_3 solution). Samples were heated overnight on a heating plate at 95°C. This operation was repeated until no more nitrous oxide (*i.e.* orange gas formed in the presence of organic matter and oxygen) could be observed.

Digested samples were diluted in 0.3 M HNO_3. Trace and minor elements were subsequently quantified using an Agilent 7900 quadrupole inductively-coupled plasma - mass spectrometer (Q-ICP-MS). Fifty-five elements were selected: Ag, Al, As, B, Ba, Be, Ca, Cd, Ce, Co, Cr, Cs, Cu, Dy, Er, Eu, Fe, Ga, Gd, Ge, Hf, Ho, K, La, Li, Lu, Mg, Mn, Mo, Nb, Nd, Ni, P, Pb, Pr, Rb, Sb, Se, Si, Sm, Sn, Sr, Ta, Tb, Th, Ti, Tl, Tm, U, V, W, Y, Yb, Zn, Zr. The same batch containing selected elements was used for all cultures to ensure similar initial elemental concentrations (Widdel and Bak, 1992). Analytical blanks were prepared simultaneously to sample preparation and their elemental content was subtracted from the measured values in samples.

To quantify the affinity of each element for MV-1 magnetite, we used the distribution coefficient (D_i for an element i) defined as:

$$D_i = \frac{C^i_{mag}}{C^i_{GM}} \qquad \text{(Eq. 1)}$$

where C^i_{mag} and C^i_{GM} correspond to the mass concentrations of the element i in grams per gram of magnetite or residual GM, respectively. Higher D_i values will reflect higher elemental incorporation and stronger affinity for magnetite. The mass of magnetite produced by MV-1 was too small to be accurately weighted. It was therefore calculated from the iron concentration measured in the purified magnetite samples. We assumed that no other form of iron was contained in the magnetite samples. Such assumption is reasonable since (1) magnetic recovery selected ferrimagnetic materials which are known to be made of magnetite only in MV-1 cultures (Bazylinski et al., 2013), (2) the magnetosome membrane, which could contain iron, was efficiently removed as confirmed by TEM characterizations, and (3) no secondary iron mineral byproducts of magnetite extraction and purification could be detected by electron microscopy, X-ray absorption spectroscopy or X-ray diffraction, as also observed in previous studies (Amor et al 2015, 2023). In the following results and discussion, we focus on the distribution coefficients for which analytical uncertainty does not exceed ± 100% of the average value. Elements with high external variability (> ±100% calculated from the two replicates) such as Be, Cs, Ta, Th or W were removed from the discussion as their incorporation into

magnetite may strongly depend on the environmental and physiological conditions, which would limit their efficiency for paleontological reconstructions.

Previous work on AMB-1 and MSR-1 showed distinct D_i values for Mn, Co and Zn which were attributed to higher Fe uptake in MSR-1 leading to Fe exhaustion in the growth medium and higher magnetite production (Amor et al, 2023). Therefore, D_i coefficients were normalized to Fe and yielded almost identical values within uncertainty, suggesting that Mn, Co and Zn partitioning does not depend on the bacterial strain when normalized to Fe. In order to compare our data obtained on MV-1 with those of AMB-1, independently of potential biases induced by culture conditions, we also used here the same partition coefficient normalized to iron (K_i):

$$K_i = \frac{D_i}{D_{Fe}} \qquad \text{(Eq. 2)}$$

In the case of higher magnetite yield, the mass of trace and minor elements contained in magnetite will increase and subsequently lead to an increase of D_i while the partition coefficient normalized to iron (K_i) should be mostly unaffected. With this notation, a partition coefficient K_i equal to 1 implies that the element *i* behaves similarly to iron, while values >1 and <1 indicate an enrichment or depletion in magnetite (relative to iron), respectively.

3. Results

3.1. Description of MV-1 cultures before cell harvesting

MV-1 bacteria were harvested after 3 to 7 days of culture, depending on the conditions tested. As explained above, the culture was stopped when the C_{mag} value reached a plateau, corresponding to an average of 4 cell cycles. From TEM observations, we observed that only 25% of the total population produced magnetosomes, with about 10 magnetite crystals per cell. Table 1 provides the bacterial concentration, the total Fe concentration and $Fe(III)/Fe_{tot}$ ratio in the residual GM at the time of MV-1 collection for all growth conditions. Bacterial concentrations ranged between 4 and 10 × 10^9 cells/mL. In all Fe(II)-ascorbate cultures, an average of 43.7 ± 7.2 µM of iron was incorporated into bacteria. It represents about 87, 56 and 33% of the 50, 100 and 150 µM of Fe initially introduced in the GM respectively. In Fe(III)-citrate cultures, initial Fe concentrations of 50 and 150 µM yielded the lowest bacterial populations (5.6 and 4.4 × 10^9 cells/mL), and Fe assimilation of only 24.3 ± 3.6 µM. In contrast, initial Fe concentration of 100 µM of Fe(III)-citrate provided the highest bacterial population

(9.6×10^9 cells/mL), with an Fe assimilation of 72.7 ± 5.9 µM. These values represent 44, 73 and 16 % of the Fe(III)-citrate initially present in the GM at 50, 100 and 150 µM, respectively. Considering the bacterial growth monitored in the various culture conditions, MV-1 cells took up similar amount of iron, with values of $5.6 \pm 1.3 \times 10^{-12}$ µmol per cell. In the residual growth medium (GM), most iron in Fe(II)-ascorbate cultures was in the form of Fe(II) while in Fe(III)-citrate cultures, GM contained a mixture of Fe(II) and Fe(III) species, with Fe(III) representing 30 to 77 % of the total dissolved Fe.

3.2. Magnetite extraction and purification

High-resolution TEM images confirmed efficient removal of the magnetosome membrane, with no organic remains observed on the purified magnetite samples (Fig. 1). Purified crystals did not show sharp edges as for instance in AMB-1 crystals (e.g. Amor et al., 2015). Identical features were observed on magnetite crystals contained in bacteria, demonstrating that the purification procedure did not alter MV-1 nanoparticles (Fig. 1). Analyses of electron diffraction patterns on extracted and purified magnetite crystals showed signs of oxidation into maghemite (γ-Fe_2O_3), identified from additional reflection spots (Fig. S3). This is likely due to air exposure and heating during sample storage and purification prior to TEM characterization. Importantly, this partial oxidation into maghemite did not impact the minor and trace element analyses that were performed on bulk samples. Finally, the length distributions of magnetite contained in MV-1, extracted from the bacteria, and purified using the TES solution were all consistent, suggesting that no magnetite material was dissolved and/or lost during sample preparation (Fig. S2).

3.3.Trace and minor element partitioning between magnetite and growth medium

The concentrations of all elements in magnetite (C^i_{mag}) and growth medium (C^i_{GM}) are reported in Table S2. Some elements analyzed in magnetite and/or residual GM after culture were either non-detectable or close to the blank level (i.e. Be, Cs, Ta, Tl, Tm, Th and W). Therefore, these elements are not further discussed. Duplicates were consistent in all culture conditions (Fig. S4). The average standard deviation between two replicates is close to 40% (RSD) with a median value around 20% (RSD). Iron distribution coefficients were variable between experimental conditions with D_{Fe} values increasing from 7.3×10^4 in 150 µM Fe(III) citrate culture up to 3.4×10^6 in 50 µM Fe(II) ascorbate culture. This can be explained by a similar mass of Fe incorporated in MV-1 cells, whatever the initial Fe concentration. The fraction of

Fe left in the residual GM thus shows large differences between growth conditions (Table 1), which resulted in variable D_i values. The distribution coefficients (D_i) between magnetite and residual GM were calculated for all elements and varied over a large range between 5.73×10^{-2} for Mg and 5.62×10^{5} for Ge (Table S3, see also Fig. 2). Only Na, Mg and K had D_i values below 1.

D_i values calculated for cultures with variable iron concentrations were compared between each other. They showed consistency for a given iron source, either Fe(II)-ascorbate or Fe(III)-citrate, and appeared relatively independent of iron concentration (Fig. 2). When plotted against each other, D_i values determined from the various Fe(II)-ascorbate concentrations showed a linear correlation with a slope close to 1. Fe(III)-citrate experiments also yielded linear correlations between D_i coefficients obtained at various initial iron concentrations, but the slopes showed lower values ranging between 0.68 and 0.82 (Fig. 2b,d,f). This variation induced by varying initial iron concentrations represents a maximum difference of 2 orders of magnitude.

Average D_i values corresponding to the two iron sources were calculated from the three conditions of initial Fe concentrations, and compared in Figure 3. They showed good agreement between D_i values in both iron source conditions, with a maximum deviation from the 1:1 line by two orders of magnitude (Ca; Fig. 3). D_{Mg} and D_K corresponded to the lowest distribution coefficients measured in MV-1 with $\log(D_i)$ values close to -0.5 and 0, respectively. In contrast, $\log(D_{Ge})$ showed values similar to Fe when MV-1 was provided with Fe(III)-citrate. Overall, these data suggest that the initial Fe redox state does not significantly influence the partition coefficients for most elements.

Contrary to D_i, the use of K_i should remain unaffected by variations in magnetosome production. Additionally, since only 25% of the MV-1 bacterial population cultivated in our study produced magnetosomes, we cannot rule out that the non-magnetic bacteria impacted the trace element budget of the growth medium, therefore changing the absolute value of distribution coefficients (D_i). A normalization to Fe (*i.e.* use of K_i value) limits this possible effect because both iron and the considered element *i* will be taken up by non-magnetic bacteria. We therefore calculated the average K_i values for MV-1 from the results obtained on all experimental conditions (Fe concentrations and redox states). The partition coefficients K_i corresponding to MV-1 and AMB-1 cultures are given in Table 2 and illustrated in Figure 4a. Only data for which standard deviation is lower than mean value are plotted. MV-1 and AMB-1 showed K_i ranging between 2×10^{-1} and 3×10^{-6} for the 25 elements. Some trace and minor elements (Ca, Cd, Co, Cr, Li, Mn, Mo, Pb, Sn, Ti, Zn) share similar behavior in the two strains,

with K_i values varying by less than one order of magnitude between the two strains. In contrast, other elements show preferential enrichment in MV-1 magnetite by more than one (Al, As, Ba, Ni, Sb, Se, Y) or two (B, Ce, Cu, La, Rb, Sr, U) orders of magnitude. Accordingly, MV-1 magnetite tends to be less pure than AMB-1 magnetite.

4. Discussion

4.1. Incorporation of trace and minor elements into MV-1 magnetite does not depend significantly on the initial iron concentration and redox state

Previous works interested in the determination of minor and trace element incorporation in MTB magnetite studied experimentally the strain AMB-1 (Amor et al., 2015) and to a lower extent MSR-1 (Amor et al, 2023), with only one fixed Fe concentration (either 100 or 150 µM) and redox state [Fe(III)]. Here we measured the concentrations of 38 elements in both MV-1 magnetite and residual GM for three initial Fe concentrations (50, 100 and 150 µM) and two redox states [Fe(II) and Fe(III)]. This work therefore enabled us to assess the variability induced by these parameters on the D_i values. The average distribution coefficients calculated in Fe(II)-ascorbate and Fe(III)-citrate conditions showed limited variability for most elements (Fig. 2 and 3). In particular, D_i values for Fe(II)-ascorbate conditions show slopes near 1 for concentrations of 50, 100 and 150 mM (Fig. 2a, c and e). For Fe(III)-citrate conditions, D_i values are also related linearly but the slopes are slightly different from 1 (Fig. 2b, d, f). This indicates a moderate dependence on Fe(III)-citrate concentration and illustrates why it is preferable to use K_i values (*i.e.* D_i normalized to D_{Fe}; Amor et al., 2015). Interestingly, Figure 3 shows that average D_i values calculated for all Fe(II)-ascorbate and Fe(III)-citrate conditions are well correlated, with a slope near 1. Over 39 elements for which D_i values could be calculated and compared for Fe(II)-ascorbate and Fe(III)-citrate conditions (Fig. 3), only 3 elements differ by more than one order of magnitude (Nd, Sr and Ca). These 3 elements are however below two orders of magnitude variations in their D_i coefficients generated by Fe(II) and Fe(III) conditions (Fig. 3; Table S3). A variation of one and in some cases two orders of magnitude is relatively small when compared to the total range of D_i values, spreading over ~6 orders of magnitude (Fig. 3). This is important for future studies on natural systems and ancient environments since MTB can thrive in a large range of geochemical conditions (Lefèvre and Bazylinski, 2013), including extreme environments (Bazylinski and Lefèvre, 2013). Our results

suggest that similar element partitioning between MTB magnetite and the extracellular solution should occur, regardless of the Fe speciation and concentration. The influence of other physico-chemical parameters such as temperature on D_i coefficients has not been explored yet and will require further studies to extend these conclusions.

4.2. Comparison of element incorporation in MV-1 and other MTB strains

The degree of metal incorporation into MTB magnetite has been examined in previous laboratory cultures under various doping conditions. For instance, MSR-1 has been cultivated at variable metal concentrations (Cu, Co, Cr, Ni, Mn and Ti) in order to produce magnetic iron spinels, $Fe_{3-x}M_xO_4$, with M being the substituting cation (Schüler and Bauerlein, 1997). However, all experiments failed since none of the crystals contained measurable amount of metals, as determined by Energy-dispersive X-ray spectroscopy (EDXS) on TEM. A latter study showed experimentally, for three *Magnetospirillum* species (MSR-1, MS-1 and AMB-1), that Co content in MTB magnetite could be increased up to 1.4% by doping the growth medium with 20 μM Co and only 5 μM of Fe (Staniland et al., 2008). Similarly, by adding dissolved Mn chloride at very high concentration (~25 mM) to uncultured MTB from a coastal lagoon, Keim et al. (2009) showed that magnetite crystals could incorporate 0.11-2.81% of Mn four days after doping. Finally, cultures of AMB-1 under metal-doping conditions (Mn, Co, Ni, Cu, Zn) showed measurable enrichment in magnetite crystals up to 2.7 % Mn, 3.0 % Co and 15.6 % Cu for initial concentrations of 1 mM, 40 μM, 20 μM respectively (Tanaka et al., 2012). Still, we note that the concentration in doping elements was artificially increased in these previous studies when compared to our experimental conditions, as growth media in our MV-1 cultures were ~ 16 μM, 2 μM and 0.1 μM for Mn, Co and Cu respectively. In addition, most of the measurements in these previous studies were performed on whole cells and integrated the elemental content of all cellular fractions (bacterial membranes, periplasm, cytosol, magnetosome membranes, magnetite…). When extracted from bacteria and purified to get rid of contamination sources, the typical range of elemental concentrations in magnetite produced by AMB-1 and MSR-1 was 1 - 100 ppm (0.0001 to 0.01 wt%) (Amor et al, 2015, 2023). Altogether, these results suggest that the organic fraction of MTB carried most of the trace and minor elements and that biological magnetite is highly depleted in doping elements. We attempted to calculate K_i values from previous studies on Mn, Co, and Cu enrichments in biomagnetite. This was only possible for the data of Staniland et al. (2008) because Co concentrations in magnetite and solution were both reported. Calculated K_{Co} estimate gives

~5.10^{-3}, a value similar to those reported for AMB-1 (1.10^{-3}) and MV-1 (2.10^{-3}) (Table 2). Overall, the content of MV-1 magnetite in minor and trace elements obtained here is consistent with that of AMB-1 and MSR-1 previously obtained (Amor et al, 2015, 2023) and previous work by Staniland et al. (2008).

Establishing trace element patterns in magnetite as a reliable biosignature of MTB requires systematic characterization of magnetite nanoparticles under physico-chemical conditions representative of natural systems, and produced by a broad variety of magnetotactic strains. Amor et al. (2015) cultivated AMB-1 by doping the growth medium in 34 elements at a low level of 100 ppb. In the present work on MV-1, trace elements were not doped at a fixed concentration value but were brought by the growth medium components (i.e. artificial seawater mixed with a modified Wolfe's mineral solution; Wolin et al., 1963; Frankel et al., 1997). All trace elements were below 250 ppb, except Mo and Co which were ~900 ppb (Table S2). Nevertheless, the average K_i values calculated for MV-1 from the results obtained here in all experimental conditions (Table 2) show that some minor and trace elements have similar behavior than that of AMB-1 (Fig. 4a). Specifically, K_i values of Ca, Cd, Co, Cr, Li, Mn, Mo, Pb, Sn, Ti and Zn vary by less than one order of magnitude between the two strains. Other elements such as Sr, Cu, U and Ce are particularly enriched in MV-1 magnetite relative to AMB-1. This comparison demonstrates that the chemical purity of MV-1 magnetite is lower than that of AMB-1 magnetite. The origin of Sr, Cu, U and Ce enrichments is unknown and such enrichments have never been reported in the literature until now. We can nevertheless speculate that MV-1 maintains higher intracellular concentrations of these elements than AMB-1, translating in a higher concentration level in magnetite. This might be due to differential properties of efflux pumps between the two strains. Importantly, K_i values for U and Ce in abiotic magnetite are equal to 1, implying that U and Ce can be favorably incorporated into magnetite if enriched in the intracellular medium. Future studies dedicated to these questions are clearly needed.

4.3. Implication for the identification of magnetofossils

The chemical purity of magnetite produced by MTB has been discussed for decades (*e.g.* Towe and Moench, 1981), and is usually considered as a reliable criterion of magnetite biogenicity (Thomas-Keprta et al., 2000). Studies on AMB-1 (Amor et al., 2015), MSR-1 (Amor et al, 2023) and MV-1 (this study) demonstrate that, although very low, trace element incorporation into MTB magnetite is measurable and different from zero. From chemical patterns of MTB (i.e., MV-1 and AMB-1 strains) and abiotic magnetite, chemical traits specific to biological

magnetite can be defined (Fig. 4 and Table 2). Consistent with previous observations on AMB-1 (Amor et al., 2015), most elements are depleted in MV-1 relative to abiotic magnetite with only seven exceptions (Al, As, B, Mo, Rb, Se and Sn) (Fig. 4b). Among these enriched elements, Mo and Sn show the best reproducibility between MV-1 and AMB-1 strains (Fig. 4a), and are clearly depleted in abiotic magnetite by two and four orders of magnitude, respectively (Fig. 4b). Accordingly, they represent promising elements for the identification of biological magnetite. The processes leading to the high affinity of molybdenum and tin for biological magnetite remain unresolved, but may result from physiological reactions. Specifically, Mo starvation in denitrifying MTB was shown to severely alter magnetite formation, as illustrated for the strain MS-1 (Taoka et al., 2003). Molybdenum serves as a metal co-factor for the nitrate reductase enzyme, which catalyzes reduction of nitrates into nitrites during denitrification reactions. In the present study, MV-1 was grown under anaerobic conditions in bottles filled with $N_2O_{(g)}$ used as a final electron acceptor (Bazylinski et al., 2013). K_i values of molybdenum were higher in AMB-1 (2×10^{-4}) than in MV-1 (2×10^{-5}) (Fig. 4). MV-1 also possesses the gene encoding for the nitrate reductase, and denitrification activity in this organism has been proposed (Bazylinski and Williams, 2007). In addition, MV-1 is capable of fixing N_2 into biomass through the activity of the nitrogenase enzyme, which also contains Mo as a co-factor (Jorgen and Bishop, 1988; Bazylinski and Williams, 2006). Even if MV-1 was cultivated under anaerobic respiration in the present study, expression of Mo-containing enzymes and subsequent increased cellular Mo demand cannot be ruled out. At first order, high Mo uptake and concentration into the cell due to metabolic demand could be translated to high Mo concentration in magnetosome and subsequently in magnetite. Finally, it was recently proposed that endogenous nitric oxide (NO), which is generated by nitrification and denitrification pathways in MTB, enhances expression of biomineralization genes and derepresses Mo-dependent denitrification processes (Pang et al, 2024). Molybdenum patterns in MTB could thus also result from complex interplays between nitrogen cycling, Mo homeostasis and magnetite biomineralization. It would be interesting to cultivate other MTB strains for which nitrogen metabolisms are not central, as for instance the sulfate-reducing *Desulfovibrio magneticus* strain RS-1 that is also able to perform fumarate and pyruvate fermentation (Sakaguchi et al., 1993). To our knowledge, a metabolic role of Sn has never been reported for MTB and remains to be explored. Tin is rarely studied in microorganisms but is considered as a moderately toxic metal (*e.g.* Pungartnik et al., 2005). However, in yeast laboratory cultures, stannous exposure was found to induce a decrease in the content of some intracellular metals (Mg, Zn, Fe), interpreted as a Sn^{2+} uptake and a competition with other

metals (Viau et al., 2012). Preferential Sn uptake in MTB might explain part of the enrichment observed in AMB-1 and MV-1 magnetite. Moreover, experiments of Sn enrichment in a bacterium isolated from a Malaysian stream water enhanced Mo reduction activity (Ghani et al., 1993). It represents an interesting prospect for a possible coupling between Sn and Mo in MTB. If Sn and Mo enrichments in magnetosome result from physiology of MTB, then these elements should also be enriched in the cellular lysate fractions containing membrane, periplasm and other organic components, or magnetosome membrane. It would be interesting to test this hypothesis by analyzing these different fractions in the future.

An intriguing observation of the present study is the strong enrichment of Ge in MV-1 magnetite (Figs. 2 and 3), which unfortunately cannot be compared to AMB-1 or to abiotic magnetite since Ge was not analyzed in our previous work (Amor et al., 2015). D_i values of Ge in MV-1 are similar to those of Fe (Fig. 2). Little is known about Ge biochemical behavior in MTB and no study reported its occurrence or significance. Germanium has two main redox states, Ge(II) and Ge(IV) (Holl et al., 2007), and is known to be incorporated in the structure of magnetite (Moon et al., 2023). Microbiological studies demonstrated that bacteria are highly tolerant to Ge, with some species able to grow with up to 1 mg/mL (Van Dyke et al., 1989; Slawson et al., 1992). Another study demonstrated that Ge could be favorably assimilated by bacteria in the presence of catechol (Chmielowski and Klapcinska, 1986), a frequent Fe-siderophore in MTB including AMB-1 (Calugay et al., 2006). The Ge cycle in MTB may thus be coupled to or driven by Fe cycling, possibly explaining the good correlation between their partition coefficients. More work is required to decipher Fe-Ge relationships in MTB.

Another group of elements corresponds to those strongly depleted in biological magnetite relative to abiotic one. This is the case for Co, Mn, Y, Sr, Ba and Pb (Fig. 4). Such depletion by two to four orders of magnitude could represent a strong indicator of magnetite biogenicity. The depletion of these elements in biogenic magnetite may indicate toxicity or limited metabolic use by magnetotactic cells. For instance, previous results on MSR-1, MS-1 and AMB-1 cultures under various Co concentrations showed that magnetosome formation was inhibited above 20 μM of Co (Staniland et al., 2008). Additionally, the bacterial growth was inhibited for Co concentrations > 200 μM. Magnetosomes with high Co content were nevertheless produced in MSR-1, MS-1 and AMB-1 by increasing the Co/Fe ratio in the growth medium (for a total metal content < 20 μM of Co; Staniland et al., 2008).

A last group of elements are characterized by similar K_i values in MTB and abiotic magnetite (plotted on or near the line 1:1 in Fig. 4b). Among these elements, Li and Ca show very consistent K_i values between MV-1 and AMB-1 magnetite. Elements such as Cr, Cd, Sb, Ti and Zn show more variability, within one order of magnitude (Fig. 4a,b). These elements can be useful for paleoenvironmental reconstruction from the rock record: since they have K_i values identical, or very close, for both biological and abiotic formation pathways, the determination of their concentration in magnetite could enable calculation of their concentrations in the fluid from which magnetite precipitated. The occurrence of magnetite in Archean or Paleoproterozoic sedimentary rocks can therefore constrain paleo-porewater or seawater concentrations of Ca, Li, Cr, Cd, Sb, Ti and Zn. Some of these elements such as Cr and Zn are critical for evaluating the redox conditions of the Earth surface (Konhauser et al., 2011; Planavsky et al., 2014; Liu et al., 2016).

Some elements show significant differences in K_i values between the two MTB strains but still hold interesting features for comparison with abiotic magnetite (Fig. 4; Table 2). For instance, both Al and Se showed stronger enrichment in MV-1 ($K_{Al} = 7 \times 10^{-2}$ and $K_{Se} = 9 \times 10^{-3}$) compared to AMB-1 ($K_{Al} = 2 \times 10^{-3}$ and $K_{Se} = 2 \times 10^{-4}$) magnetite, but are two to three orders of magnitude higher relative to abiotic magnetite ($K_{Al} = 5.10^{-5}$ and $K_{Se} = 3.10^{-6}$). In addition, Ba, U and Sr were strongly enriched in MV-1 ($K_{Ba} = 8.10^{-3}$, $K_U = 2.10^{-1}$ and $K_{Sr} = 6.10^{-3}$) relative to AMB-1 ($K_{Ba} = 7.10^{-4}$, $K_U = 1.10^{-4}$ and $K_{Sr} = 1.10^{-5}$) by more than two orders of magnitude. It must be emphasized that U is highly enriched in abiotic magnetite with $K_{abiotic}$ values of ~1, implying a behavior similar to Fe (Fig. 4b). Given its large depletion in AMB-1 magnetite, the partitioning of Sr between AMB-1 magnetite and growth medium was previously suggested to represent a promising tracer of MTB magnetite when combined with Ca (Amor et al., 2015). The K_{Sr}/K_{Ca} ratio showed a variation of 5 orders of magnitude between AMB-1 (3×10^{-2}) and abiotic magnetite (10^3) (Amor et al, 2015). A literature survey shows that partitioning of Sr normalized to Ca during precipitation of Ca carbonates does not strongly depend on chemical conditions, with a variation of one order of magnitude at most. Accordingly, the Sr/Ca ratio of a solution from which magnetite precipitates could be reconstructed from associated Ca carbonates with a precision sufficient for determining the origin of magnetite. However, data obtained here showed that MV-1 magnetite was less depleted in Sr than that of AMB-1, with a K_{Sr}/K_{Ca} of 30 that may not be easily distinguished from abiotic magnetite given the variation of Sr partitioning in Ca carbonates. A similar approach could be defined by selecting distinct

elements more appropriate for both AMB-1 and MV-1. Relevant ratios for calculation of the fluid composition could be for instance Co/Zn, Pb/Zn and Mn/Zn in sulfides, and Mn/Ca in carbonates. This approach would imply the assumption that carbonates and sulfides formed from the same fluid as magnetite which could be tested in parallel by using the ratio of two elements with close K_i values for MTB and abiotic magnetite (i.e. Li/Ca). If applicable, then the fluid Li/Ca ratios predicted from magnetite, sulfide and carbonate should give similar values. This method will need to be examined in the future on natural rock samples.

The determination of magnetofossils in ancient rock samples should rely on multiple techniques not only based on trace element content. First, magnetic characterization (First-Order Reversal Curve (FORC), Verwey transition temperature) could help to identify and select the most appropriate samples, with the highest chance to contain magnetofossils (*e.g.* Helsop et al., 2014; Chang et al., 2016). Then, a careful petrological and mineralogical work using microscopy techniques would define the various types of magnetite, their size, shape, associations between them and with other minerals, as well as their precise location in the rock samples. Finally, bulk magnetite in well-identified zones should be separated either chemically and/or magnetically before dissolution and analyses by ICP-MS. *In situ* analysis of minor and trace elements content in single magnetite particles is still not possible due to their small size (i.e. <100 nm) but the development of new techniques such as Atome Probe Tomography (APT), with nm scale-resolution, is very promising (Reddy et al., 2020).

To summarize, we highlight that magnetofossils in ancient sedimentary rocks could be identified from their enrichment in Mo and Sn, as well as Se and Al. Strong depletion is expected in Co, Mn and Pb relative to abiotic magnetite. In contrast, elements such as Ca or Li are expected to be similar in abiotic and MTB magnetite and could be used as normalization means to overcome limitation of fluid accessibility. This work thus further establishes the use of elemental ratios in a population of magnetite crystals as a promising chemical tool for identification of magnetofossils. Before using these chemical proxies to search traces of MTB in ancient terrestrial and extraterrestrial rock samples, the present conclusions should be tested in modern natural environments where both MTB and associated waters can be sampled. This should be possible thanks to recent improvement in the efficiency of MTB collection in natural systems (Busigny et al., 2021).

5. Conclusion and perspectives

MV-1 and AMB-1 are two different MTB strains living in marine and freshwater environments, respectively. These bacteria have been isolated from different aquatic habitats, have different metabolisms and synthesize different magnetite nanocrystals of elongated-prismatic or cuboctahedral shapes, respectively. The patterns of trace and minor element incorporation in the magnetite produced by these two strains share striking similarities, while they both have marked differences with abiotic magnetite. This suggests that magnetite from all MTB are probably chemically distinguishable from abiotic ones. Such patterns are attributed to bacterial metabolic activity and biological control on the internal cellular medium (Amor et al, 2022). Biomagnetite precipitates in a strictly controlled environment within the magnetosome vesicles. If such minor and trace element patterns can be extended to all MTB, it could provide a powerful tool for defining a biosignature of magnetofossils. Both AMB-1 and MV-1 belong to the *Alphaproteobacteria* class of the *Pseudomonadota* phylum (Lefèvre and Bazylinski, 2013; Goswami et al., 2022) and were grown in conditions where the cells used nitrogenous compounds as terminal electron acceptors. It would be interesting to investigate the chemical composition of magnetite produced by distinct strains belonging to other taxa, such as the sulfate-reducing or fermentative *Desulfovibrio magneticus* strain RS-1 affiliated to the *Desulfobacterota* phylum, and test the general applicability of the criteria proposed here, especially those related to molybdenum enrichment in magnetite. Finding reproducible patterns within a single taxon or eventually among various taxa could help to better understand the origin and evolution of MTB.

In the future, it will be important to explore the minor and trace element signatures of MTB in natural environments to determine if conclusions derived from laboratory experiments on AMB-1 and MV-1 can be translated to natural systems. Recent work on anoxic and ferruginous Lake Pavin, France, demonstrated our capability to collect high amount of MTB near the redox transition zone of the water column (Busigny et al., 2021), limiting the risk of magnetic contaminants and thus paving the way for future trace element measurements of MTB magnetite concomitantly with water samples.

Finally, it should be emphasized that chemical signature based on minor and trace elements concentration alone is not sufficient to establish the biogenicity of magnetite. Future studies should combine this approach to morphological (size distribution and specific morphologies using microscopic observations) and magnetic criteria (Thomas-Keprta et al., 2000; Heslop et al., 2014; Chang et al., 2016) to better identify biomagnetite in the rock record.

CRediT authorship contribution statement

François P. Mathon: Investigation, Formal analysis, Visualization, Writing – original draft. **Matthieu Amor:** Methodology, Validation, Writing – review & editing. **François Guyot:** Conceptualization, Methodology. **Nicolas Menguy:** Methodology, Resources. **Vincent Busigny and Christophe Lefèvre:** Conceptualization, Funding acquisition, Methodology, Project administration, Resources, Supervision, Validation, Writing – review & editing.

Appendix A. Supplementary material

Supplementary material includes a file with four figures illustrating the monitoring of MV-1 cultures (Fig. S1), histograms of size distribution of magnetite nanocrystals produced by MV-1 at all steps of our analytical procedure (Fig. S2), TEM diffraction pattern of magnetosome showing partial oxidation to maghemite (Fig. S3), a comparison of the distribution coefficients calculated from replicate analyses (Fig. S4), as well as three tables reporting the parameters monitored during MV-1 cultures (Table S1), trace element compositions of magnetite and final growth medium (Table S2) and the average distribution coefficients between magnetite and growth medium for all culture conditions (Table S3).

Acknowledgments

Colleagues from the stable isotope laboratory and BIAM-CEA Cadarache are thanked for help and discussions. This work was supported by the French National Research Agency (SIGMAG: ANR-18-CE31-0003 and BIOMAG: ANR-23-CE49-0007) and the Institut de Physique du Globe de Paris. V.B. thanks the Institut Universitaire de France (IUF#2017-2021) and INSU-CNRS Origines program (AAP2023) for funding. Part of this work was supported by IPGP multidisciplinary program PARI and by Région Île-de- France SESAME Grant no. 1015908. MA is supported by grant through the CNRS TelluS/INTERRVIE program (grant #MagBio). We thank Pierre Burckel and Samia Hidalgo for analytical assistance in ICP-QMS measurements.

References

Akai J., Iida A., Akai K., Chiba A.,1997. Mn and Fe Minerals of Possible Biogenic Origin from Two Precambrian Stromatolites in Western Australia. *The Journal of the Geological Society of Japan* 103, 484–88.

Amor M., Busigny V., Louvat P., Gelabert A., Cartigny P., Durand-Dubief M., Ona-Nguema G., Alphandery E., Chebbi I., Guyot F., 2016. Mass-Dependent and -Independent Signature of Fe Isotopes in Magnetotactic Bacteria. *Science* 352, 705–708.

Amor M., Busigny V., Durand-Dubief M., Tharaud M., Ona-Nguema G., Gelabert A., Alphandery E., Menguy N., Benedetti M., Chebbi I., Guyot F., 2015. Chemical Signature of Magnetotactic Bacteria. *Proceedings of the National Academy of Sciences* 112, 1699–1703.

Amor M., Mathon F.P., Monteil C.L., Busigny V., Lefevre C.T., 2020. Iron-biomineralizing Organelle in Magnetotactic Bacteria: Function, Synthesis and Preservation in Ancient Rock Samples. *Environmental Microbiology* 22, 3611–32.

Amor M., Tharaud M., Gélabert A., Komeili A., 2020. Single-cell Determination of Iron Content in Magnetotactic Bacteria: Implications for the Iron Biogeochemical Cycle. *Environmental Microbiology* 22, 823–31.

Amor M., Faivre D., Corvisier J., Tharaud M., Busigny V., Komeili A., Guyot F., 2022. Defining Local Chemical Conditions in Magnetosomes of Magnetotactic Bacteria. *Journal of Physical Chemistry B* 126, 2677-2687.

Amor M., Mosselmans J.F.W., Scoppola E., Li C., Faivre D., Chevrier D.M., 2023. Crystal-chemical and biological controls of elemental incorporation into magnetite nanocrystals. *ACS Nano* 17, 927-939.

Arato B., Szanyi Z., Flies C., Schüler D., Frankel R.B., Buseck P.R., Posfai M., 2005. Crystal-size and shape distributions of magnetite from uncultured magnetotactic bacteria as a potential biomarker. *American Mineralogist* 90, 1233–1240.

Baumgartner J., Morin G., Menguy N., Gonzalez T.P., Widdrat M., Cosmidis J., Faivre D., 2013. Magnetotactic bacteria form magnetite from a phosphate-rich ferric hydroxide via nanometric ferric (oxyhydr)oxide intermediates. *Proc. Natl. Acad. Sci. U. S. A.* 110, 14883–14888.

Bazylinski D.A., Frankel R.B., 2004. Magnetosome Formation in Prokaryotes. *Nature Reviews Microbiology* 2, 217–30.

Bazylinski D.A., Williams T.J., 2007. Ecophysiology of magnetotactic bacteria. In *magnetoreception and magnetosomes in bacteria*., Eds D. Schüler, 37-75. Berlin, Heidelberg.

Bazylinski D.A., Moskowitz B.M., 1997. Chapter 6. Microbial biomineralization of magnetic iron minerals: microbiology, magnetism and environmental significance. In *Geomicrobiology*, Eds J.F. Banfield and K.H. Nealson, 181–224. Berlin, Boston: De Gruyter.

Bazylinski D.A., Lefèvre C.T., 2013. Magnetotactic bacteria from extreme environments. Life (Basel) 3, 295-307.

Bazylinski D.A., Williams T.J., Lefèvre C.T., Trubitsyn D., Fang J., Beveridge T.J., Moskowitz B.M., Ward B., Schübbe S., Dubbels B.L., Simpson B., 2013. Magnetovibrio blakemorei gen. nov., sp. nov., a magnetotactic bacterium (Alphaproteobacteria: Rhodospirillaceae) isolated from a salt marsh. *International Journal of Systematic and Evolutionary Microbiology* 63, 1824–33.

Bidaud C.C., Monteil C.L., Menguy N., Busigny V., Jézéquel D., Viollier E., Travert C., Skouri-Panet F., Benzerara K., Lefevre C.T., Duprat E., 2022. Biogeochemical Niche of Magnetotactic Cocci Capable of Sequestering Large Polyphosphate Inclusions in the Anoxic Layer of the Lake Pavin Water Column. Frontiers in Microbiology 12, 789134.

Buseck P.R., Dunin-Borkowski R.E., Devouard B., Franke R.B., McCartney M.R., Midgley P.A., Posfai M., Weyland M., 2001. Magnetite morphology and life on Mars. *Proceedings of the National Academy of Sciences of America* 98, 13490-13495.

Busigny V., Mathon F.P., Jézéquel D., Bidaud C., Viollier E., Bardoux G., Bourrand J.-J., Benzerara K., Duprat E., Menguy N., Monteil C.L., Lefevre C.T., 2021. Mass collection of magnetotactic bacteria from the permanently stratified ferruginous Lake Pavin, France. *Environmental Microbiology* 24, 721-736.

Calugay R.J., Takeyama H., Mukoyama D., Fukuda Y., Suzuki T., Kanoh K., Matsunaga T., 2006. Catechol siderophore excretion by magnetotactic bacterium *Magnetospirillum magneticum* AMB-1. *J. Biosci. Bioeng.* 101, 445-447.

Chang L., Heslop D., Roberts A.P., Rey D., Mohamed K.J., 2016. Discrimination of Biogenic and Detrital Magnetite through a Double Verwey Transition Temperature. *Journal of Geophysical Research: Solid Earth* 121, 3–14.

Chang L., Harrison R.J., Zeng F. Berndt T.A., Roberts AP., Heslop D., Zhao X., 2018. Coupled microbial bloom and oxygenation decline recorded by magnetofossils during the Palaeocene–Eocene Thermal Maximum. *Nature Communication* 9, 4007.

Chang S.B.R., Kirschvink J.L., 1989. Magnetofossils, the Magnetization of Sediments, and the Evolution of Magnetite Biomineralization. *Annual Review of Earth and Planetary Sciences* 17, 169–95.

Chmielowski J., Klapcinska B. 1986. Bioaccumulation of germanium by Pseudomonas putida in the presence of two selected substrates. *Appl. Environ. Microbial.* 51, 1099-l103.

Devouard B., Posfai M., Hua X., Bazylinski D.A., Frankel R.B., Buseck P.R., 1998. Magnetite from Magnetotactic Bacteria; Size Distributions and Twinning. *American Mineralogist* 83, 1387–98.

Dong Y., Li J., Zhang W., Zhao Y.., Xiao T., Wu L.-F., Pan H., 2016. The detection of magnetotactic bacteria in deep sea sediments from the east Pacific Manganese Nodule Province. *Environmental Microbiology Reports* 8, 239-249.

Egli R., 2004. Characterization of Individual Rock Magnetic Components by Analysis of Remanence Curves. 3. Bacterial Magnetite and Natural Processes in Lakes. *Physics and Chemistry of the Earth, Parts A/B/C* 29 (13–14), 869–84.

Faivre D., Zuddas P., 2006. An Integrated Approach for Determining the Origin of Magnetite Nanoparticles. *Earth and Planetary Science Letters* 243, 53–60.

Faivre D., Schüler D., 2008. Magnetotactic Bacteria and Magnetosomes. *Chemical Reviews* 108, 4875–98.

Flies C.B., Jonkers H.M., de Beer D., Bosselmann K., Böttcher M.E., Schüler D., 2005. Diversity and vertical distribution of magnetotactic bacteria along chemical gradients in freshwater microcosms. *FEMS Microbiol Ecol.* 52, 185-95.

Frankel R.B., Papaefthymiou G.C., Blakemore R.P., O'Brien W., 1983. Fe_3O_4 precipitation in magnetotactic bacteria. *Biochim. Biophys. Acta* 763, 147–159.

Frankel R.B., Bazylinski D.A., Johnson M.S., Taylor B.L., 1997. Magneto-Aerotaxis in Marine Coccoid Bacteria. *Biophysical Journal* 73, 994–1000.

Ghani B., Takai M., Hisham N.Z., Kishimoto N., Ismail A. K.M., Tano T., Sugio T., 1993. Isolation and characterization of a Mo^{6+}-reducing bacterium. *Appl. Environ. Microbiol.* 59, 1176–1180.

Ginet N., Pardoux R., Adryanczyk G., Garcia D., Brutesco C., Pignol D., 2011. Single-Step Production of a Recyclable Nanobiocatalyst for Organophosphate Pesticides Biodegradation Using Functionalized Bacterial Magnetosomes. Edited by F. Rodrigues-Lima. *PLoS ONE* 6 (6): e21442.

Goswami P., He K., Li J., Pan Y., Roberts A.P., Lin W., 2022. Magnetotactic bacteria and

magnetofossils: ecology, evolution and environmental implications. *NPJ Biofilms and Microbiomes* 8:43.

Havas R., Savian J.F., Busigny V., 2021. Iron isotope signature of magnetofossils and oceanic biogeochemical changes through the Middle Eocene Climatic Optimum. *Geochimica et Cosmochimica Acta* 311, 332-352

Heslop D., Roberts A.P., Chang L., 2014. Characterizing Magnetofossils from First-Order Reversal Curve (FORC) Central Ridge Signatures. *Geochemistry, Geophysics, Geosystems* 15, 2170–79.

Höll R., Kling M., Schroll E., 2007. Metallogenesis of germanium – A review. *Ore Geology Reviews* 30, 145-180.

Joerger R.D., Bishop P.E., 1988. Bacterial alternative nitrogen fixation systems. *CRC Crit. Rev. Microbiol.* 16, 1 –14.

Jogler C., Niebler M., Lin W., Kube M., Wanner G., Kolinko S., Stief P., Beck A.J., De Beer D., Petersen N., Pan Y., Amann R., Reinhardt R., Schüler D., 2010. Cultivation-independent characterization of 'Candidatus Magnetobacterium bavaricum' via ultrastructural, geochemical, ecological and metagenomic methods. *Environ. Microbiol.* 12, 2466-78.

Keim C.N., Lins U., Farina M., 2009. Manganese in biogenic magnetite crystals from magnetotactic bacteria. *FEMS Microbiol. Lett.* 292, 250–253.

Keshoju K, Xing H., Sun L., 2007. Magnetic field driven nanowire rotation in suspension. Applied Physics Letters 91, 123114.

Klein C., 2005. Some Precambrian Banded Iron-Formations (BIFs) from around the World: Their Age, Geologic Setting, Mineralogy, Metamorphism, Geochemistry, and Origins. *American Mineralogist* 90, 1473–99.

Konhauser K.O., Lalonde S.V., Planavsky N.J., Pecoits E., Lyons T.W., Mojzsis S.J., Rouxel O.J., Barley M.E., Rosìere C., Fralick P.W., Kump L.R., Bekker A., 2011. Aerobic bacterial pyrite oxidation and acid rock drainage during the Great Oxidation Event. *Nature* 478, 369-373.

Kopp R. E., Kirschvink J.L., 2008. The Identification and Biogeochemical Interpretation of Fossil Magnetotactic Bacteria. *Earth-Science Reviews* 86, 42–61.

Le Nagard L., Zhu X., Yuan H., Benzerara K., Bazylinski D.A., Fradina C., Besson A., Swaraj S., Stanescu S., Belkhou R., Hitchcock A.P., 2019. Magnetite magnetosome biomineralization in Magnetospirillum magneticum strain AMB-1: A time course study. *Chemical Geology* 530, 119348.

Lefèvre C.T., Frankel R.B., Abreu F., Lins U., Bazylinski D.A., 2011. Culture-independent characterization of a novel, uncultivated magnetotactic member of the Nitrospirae phylum. *Environ. Microbiol.* 13, 538-49.

Lefèvre C.T., Bazylinski D.A., 2013. Ecology, Diversity, and Evolution of Magnetotactic Bacteria. *Microbiology and Molecular Biology Reviews* 77, 497–526.

Lefèvre C.T., Trubitsyn D., Abreu F., Kolinko S., Jogler S., Almeida L.G., de Vasconcelos A.T., Kube M., Reinhardt R., Lins U., Pignol D., Schüler D., Bazylinski D.A., Ginet N., 2013. Comparative genomic analysis of magnetotactic bacteria from the *Deltaproteobacteria* provides new insights into magnetite and greigite magnetosome genes required for magnetotaxis. *Environmental Microbiology* 15, 2712-2735.

Lefèvre C.T., Wu. L.F., 2013. Evolution of the Bacterial Organelle Responsible for Magnetotaxis. *Trends in Microbiology* 21, 534–43.

Lin W., Paterson G.A., Zhu Q., Wang Y., Kopylova E., Li Y., Knight R., Bazylinski D.A., Zhuh R., Kirschvink J.L., Pan Y., 2017. Origin of Microbial Biomineralization and Magnetotaxis during the Archean. *Proceedings of the National Academy of Sciences* 114, 2171–76.

Li J., Zhang H., Liu P., Menguy N., Roberts A.P., Chen H., Wang Y., Pan Y., 2019. Phylogenetic and structural identification of a novel magnetotactic Deltaproteobacteria strain, WYHR-1, from a freshwater lake. *Appl. Environ. Microbiol.* 85 (14), e00731-19.

Liu X.M., Kah L.C., Knoll A.H., Cui H., Kaufman A.J., Shahar A., Hazen R.M., 2016. Tracing Earth's O_2 evolution using Zn/Fe ratios in marine carbonates. *Geochem. Persp. Let.* 2, 24-34.

Liu P., Liu Y., Zhao X., Roberts A.P., Zhang H., Zheng Y., Wang F., Wang L., Menguy N., Pan Y., Li J., 2021a. Diverse Phylogeny and Morphology of Magnetite Biomineralized by Magnetotactic Cocci. *Environmental Microbiology* 23, 1115-1129.

Liu P., Tamaxia A., Liu Y., Qiu H., Pan J., Jin Z., Zhao X., Roberts A.P., Pan Y., Li J., 2021b. Identification and characterization of magnetotactic Gammaproteobacteria from a salt evaporation pool, Bohai Bay, China. *Environmental Microbiology* 24, 938-950.

Mathon, F., 2021. Signature des magnétites produites par les bactéries magnétotactiques : perspectives chimiques et isotopiques. PhD Université Paris Cité, Paris, France, 338 pp.

Matsunaga T., Sakaguchi T., Tadakoro F., 1991. Magnetite Formation by a Magnetic Bacterium Capable of Growing Aerobically. *Applied Microbiology and Biotechnology* 35, 651-655.

Mériaux S., Boucher M., Marty B., Lalatonne Y., Prévéral S., Motte L., Lefèvre C.T., Geffroy F., Lethimonnier F., Péan M., Garcia D., Adryanczyk-Perrier G., Pignol D., Ginet N., 2015. Magnetosomes, Biogenic Magnetic Nanomaterials for Brain Molecular Imaging with 17.2 T MRI Scanner. *Advanced Healthcare Materials* 4, 1076–1083.

Monteil C.L., Benzerara K., Menguy N., Bidaud C., Michot-Achdjian E., Bolzoni R., Mathon F., Coutaud M., Alonso B., Garau C., Jézéquel D., Viollier E., Ginet N., Floriani M., Swaraj S., Sachse M., Busigny V., Duprat E., Guyot F., Lefevre C.T., 2021. Intracellular amorphous Ca-carbonate and magnetite biomineralization by a magnetotactic bacterium affiliated to the Alphaproteobacteria. *ISME Journal* 15, 1-18.

Moon I., Liu L., Yang X., Suh Y.J., Jung J., Ha, Y, 2023. Chemical signatures of Ge in magnetite of Wugang BIF, China. *Appl. Sci.* 13, 8246.

Pang B., Zheng H., Ma S., Tian J., Wen Y., 2024. Nitric oxide sensor NsrR is the key direct regulator of magnetosome formation and nitrogen metabolism in Magnetospirillum. *Nucleic Acids Research*, 1–18.

Planavsky N.J., Reinhard C.T., Wang X., McGoldrick P., Thompson D., Rainbird R.H., Fischer W., Johnson T.M., Lyons T.W., 2014. Low Mid-Proterozoic atmospheric oxygen levels and the delayedrise of animals. *Science* 346, 635-638.

Pungartnik, C., Viau, C., Picada, J., Caldeira-de-Araújo, A., Henriques, J.A.P., Brendel, M., 2005. Genotoxicity of stannous chloride in yeast and bacteria. *Mutat. Res.* 583, 146–157.

Reddy S.M., Saxey D.W., Rickard W.D.A., Fougerousse D., Montalvo S.D., Verberne R., van Riessen A., 2020. Atom Probe Tomography: Development and Application to the Geosciences. *Geostandards and Geoanalytical Research* 44, 5-50.

Roberts A.P., Florindo F., Villa G., Chang L., Jovane L., Bohaty S. M., Larrasoana J. C., Heslop D., Fitz Gerald J. D., 2011. Magnetotactic bacterial abundance in pelagic marine environments is limited by organic carbon flux and availability of dissolved iron. *Earth Planet. Sci. Lett.* 310, 441–452.

Sakaguchi T., Burgess J.G., Matsunaga T., 1993. Magnetite formation by a sulphate-reducing bacterium. *Nature* 365, 47-49.

Schüler D., 2006. Biochemical and Genetic Analysis of the Magnetosome Membrane in Magnetospirillum Gryphiswaldense. In *Biomineralization: From Biology to Biotechnology and Medical Application,* edited by E. Baeuerlein, pp. 61-72. Wiley-VCH, Weinheim, Germany.

Schüler D., Köhler M., 1992. The isolation of a new magnetic spirillum. *Zentralbl. Mikrobiol.* 147, 150-151

Schüler D., Uhl R., Bäuerlein E., 1995. A Simple Light Scattering Method to Assay Magnetism in *Magnetospirillum Gryphiswaldense*. *FEMS Microbiology Letters* 132, 139–145.

Schüler D., Baeuerlein E., 1998. Dynamics of iron uptake and Fe_3O_4 biomineralization during aaerobic and microaerobic growth of *Magnetospirillum gryphiswaldense*. *Journal of Bacteriology* 180, 159-162.

Slawson R.M., Van Dyke M.I., Lee H., Trevors J.T., 1992. Germanium and silver resistance, accumulation, and toxicity in microorganisms. *Plasmid* 27, 72-79.

Staniland S., Williams W., Telling N., Van Der Laan G., Harisson A., Wardi B., 2008. Controlled cobalt doping of magnetosomes in vivo. *Nature Nanotechnol* 3, 158–162.

Tanaka M., Brown R., Hondow N., Arakaki A., Matsunaga T., Staniland S., 2012. Highest levels of Cu, Mn and Co doped into nanomagnetic magnetosomes through optimized biomineralisation. *J. Mater. Chem.* 22, 11919–11921.

Taoka A., Yoshimatsu K., Kanemori M., Fukumori Y., 2003. Nitrate Reductase from the Magnetotactic Bacterium *Magnetospirillum Magnetotacticum* MS-1: Purification and Sequence Analyses. *Canadian Journal of Microbiology* 49, 197–206.

Thomas-Keprta K.L., Bazylinski D.A., Kirschvink J.L., Clemett S.J., McKay D.S., Wentworth S.J., Vali H., Gibson E.K., Romanek C.S., 2000. Elongated Prismatic Magnetite Crystals in ALH84001 Carbonate Globules. *Geochimica et Cosmochimica Acta* 64, 4049–4081.

Thomas-Keprta K.L., Clemett S.J., McKay D.S., Gibson E.K., Wentworth S.J., 2009. Origins of Magnetite Nanocrystals in Martian Meteorite ALH84001. *Geochimica et Cosmochimica Acta* 73, 6631–6677.

Towe K., Moench T.T., 1981. Electron-optical characterization of bacterial magnetite. *Earth Planet. Sci. Lett.* 52, 213–220.

Uebe R., Schüler D., 2016. Magnetosome Biogenesis in Magnetotactic Bacteria. *Nature Reviews Microbiology* 14, 621–37.

Van Dyke M.I., Lee H., Trevors, J.T. 1989. Germanium toxicity in selected bacterial and yeast strains. *J. Ind. Microbial.* 4, 299-306.

Viau C.M., Cardone J.M., Guecheva T.N., Yoneama M.-L., Dias J.F., Pungartnik C., Brendel M., Saffi

J., Henriques J.A.P., 2012. Enhanced resistance of yeast mutants deficient in low-affinity iron and zinc transporters to stannous-induced toxicity. *Chemosphere* 86, 477-484.

Viollier E., Inglett P.W., Hunter K., Roychoudhury A.N., Van Cappellen P., 2000. The Ferrozine Method Revisited: Fe(II)/Fe(III) Determination in Natural Waters. *Applied Geochemistry* 15, 785–90.

Widdel F., Bak F., 1992. Gram-Negative Mesophilic Sulfate-Reducing Bacteria. In *The Prokaryotes*, edited by A. Balows, H., Trüper, M. Dworkin, W. Harder, K.-H. Schleifer, 3352–3378. New York, NY: Springer New York.

Wolin E.A., Wolin M.J., Wolfe R.S., 1963. Formation of methane by bacterial extracts. *J. Biol. Chem.* 238, 2882-2886.

Zhu X.H., Hitchcock A.P., Bazylinski D.A., Denes P., Joseph J., Lins U., Marchesini S., Shiu H.-W., Tyliszczak T., Shapiro D.A., 2016. Measuring spectroscopy and magnetism of extracted and intracellular magnetosomes using soft X-ray ptychography. *Proc. Natl. Acad. Sci. U. S. A.* 113, E8219–E8227.

Table 1
Final bacterial populations, Fe concentration and redox ratio (Fe(III)/Fe(II)+Fe(III)) measured in the growth media when harvesting MV-1 cells, for all replicate and culture conditions tested here.

Iron source	Fe(II)-ascorbate						Fe(III)-citrate					
	50 µM		100 µM		150 µM		50 µM		100 µM		150 µM	
Replicate	#1	#2	#1	#2	#1	#2	#1	#2	#1	#2	#1	#2
Final population ($\times 10^9$ cells/mL)	6.2	6.3	8.7	8.4	7.9	8.2	6.8	5.6	9.3	9.6	6.0	4.4
$[Fe_{total}]$ (μM)	6	5	35	34	109	103	29	32	30	24	125	132
$\frac{[Fe(III)]}{[Fe_{total}]}$ (%)	4.5	5.4	3.5	3.7	8.2	6.4	30.1	29.8	65.5	66.3	75.6	77.3

NB: bacterial population were estimated by optical density (OD 560 nm) measurement, Fe concentrations by ferrozine assays (total remaining iron after bacterial growth was later determined by ICP-QMS), low [Fe(III)] measured by ferrozine assay on the GM containing Fe(II)-ascorbate were negligible and may be due to iron oxidation during the measurement process. Incubation time was at least 10 min for Fe(II) measurement, implying that the growth medium was exposed to air conditions and could be oxidized by ambient O_2.

Table 2
Partition coefficients between magnetite and solution (normalized to iron) for abiotic precipitation ($K_{abiotic}$), and cultures of AMB-1 (K_{AMB-1}) and MV-1 (K_{MV-1}) strains.

Element	$K_{abiotic}$ *	± 1SD	K_{AMB-1} *	± 1SD	K_{MV-1}	± 1SD
Al	5.0×10^{-5}	2.0×10^{-6}	2.0×10^{-3}	1.0×10^{-3}	6.7×10^{-2}	2.2×10^{-2}
As	2.0×10^{-4}	1.0×10^{-4}	2.0×10^{-4}	1.0×10^{-4}	1.4×10^{-2}	6.5×10^{-3}
B	1.0×10^{-4}	2.0×10^{-4}	2.0×10^{-5}	2.0×10^{-5}	4.6×10^{-3}	1.1×10^{-3}
Ba	4.0×10^{-1}	4.0×10^{-1}	7.0×10^{-4}	5.0×10^{-4}	7.7×10^{-3}	8.8×10^{-4}
Ca	2.0×10^{-4}	3.0×10^{-6}	5.0×10^{-4}	3.0×10^{-4}	2.1×10^{-4}	1.6×10^{-4}
Cd	9.0×10^{-3}	3.0×10^{-4}	2.0×10^{-5}	1.0×10^{-6}	2.7×10^{-3}	1.4×10^{-4}
Ce	1.0×10^{0}	1.0×10^{-1}	2.0×10^{-4}	2.0×10^{-4}	2.3×10^{-1}	2.6×10^{-2}
Co	1.0×10^{0}	5.0×10^{-1}	1.0×10^{-3}	1.0×10^{-4}	2.1×10^{-3}	3.6×10^{-5}
Cr	2.0×10^{-1}	5.0×10^{-3}	1.0×10^{-2}	6.0×10^{-3}	5.4×10^{-2}	1.1×10^{-3}
Cu	9.0×10^{-2}	5.0×10^{-2}	9.0×10^{-5}	2.0×10^{-5}	1.3×10^{-1}	4.6×10^{-3}
La	1.0×10^{0}	3.0×10^{-2}	2.0×10^{-4}	2.0×10^{-4}	9.7×10^{-2}	7.8×10^{-3}
Li	8.0×10^{-5}	3.0×10^{-6}	2.0×10^{-5}	2.0×10^{-6}	3.3×10^{-5}	9.4×10^{-6}
Mn	1.0×10^{0}	5.0×10^{-2}	2.0×10^{-3}	1.0×10^{-4}	4.0×10^{-4}	9.0×10^{-5}
Mo	4.0×10^{-7}	1.0×10^{-7}	1.0×10^{-4}	7.0×10^{-5}	2.6×10^{-5}	3.5×10^{-6}
Ni	2.0×10^{-1}	7.0×10^{-2}	5.0×10^{-4}	1.0×10^{-4}	1.7×10^{-2}	8.4×10^{-4}
Pb	5.0×10^{-1}	2.0×10^{-1}	1.0×10^{-3}	6.0×10^{-4}	5.4×10^{-3}	1.4×10^{-4}
Rb	1.0×10^{-6}	3.0×10^{-8}	3.0×10^{-6}	5.0×10^{-7}	2.1×10^{-4}	1.1×10^{-5}
Sb	1.0×10^{-2}	1.0×10^{-3}	8.0×10^{-4}	4.0×10^{-5}	9.7×10^{-3}	1.8×10^{-3}
Se	3.0×10^{-6}	5.0×10^{-7}	2.0×10^{-4}	4.0×10^{-5}	8.6×10^{-3}	4.9×10^{-3}
Sn	6.0×10^{-7}	2.0×10^{-8}	5.0×10^{-3}	3.0×10^{-3}	3.3×10^{-3}	2.6×10^{-4}
Sr	2.0×10^{-1}	3.0×10^{-3}	1.0×10^{-5}	1.0×10^{-6}	5.6×10^{-3}	9.6×10^{-5}
Ti	6.0×10^{-2}	2.0×10^{-2}	5.0×10^{-3}	3.0×10^{-3}	2.8×10^{-2}	1.3×10^{-2}
U	1.0×10^{0}	2.0×10^{-1}	1.0×10^{-4}	5.0×10^{-5}	1.5×10^{-1}	1.3×10^{-2}
Y	1.0×10^{0}	2.0×10^{-2}	1.0×10^{-4}	1.0×10^{-4}	7.0×10^{-3}	2.3×10^{-3}
Zn	2.0×10^{-2}	8.0×10^{-3}	8.0×10^{-4}	6.0×10^{-5}	4.7×10^{-3}	1.0×10^{-4}

* Data on abiotic and AMB-1 magnetite from Amor et al. (2015).

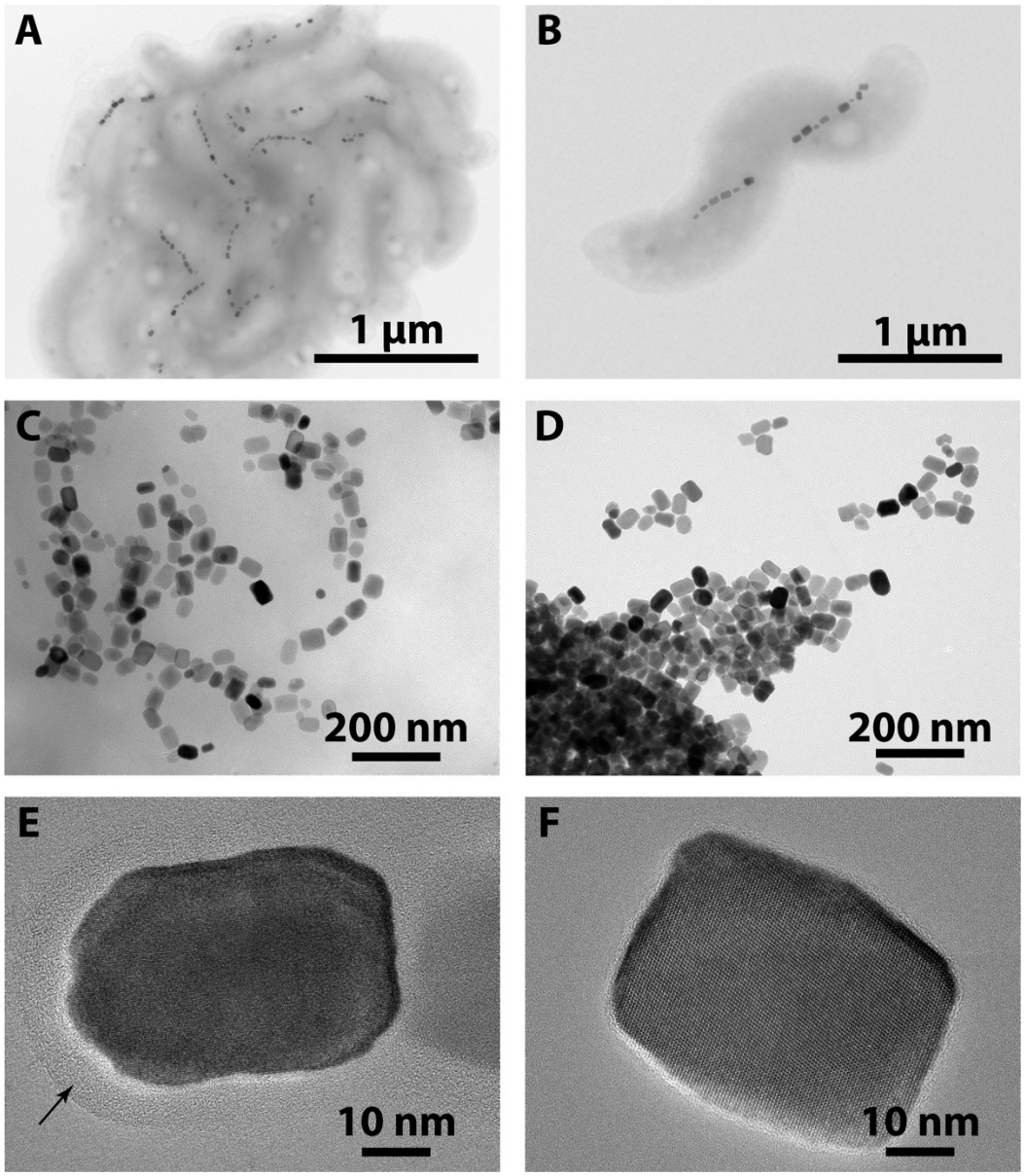

Fig. 1. Transmission electron microscopy (TEM) images representative of MV-1 cells and their magnetosomes observed from bottle cultures to purified single nanocrystals of magnetite. (A) Aggregate of MV-1 cells and their magnetic chain (*i.e.* dark chains of nanocrystals). (B) Single MV-1 cell exhibiting a unique chain of magnetosomes with a central part deprived of magnetite. (C) Extracted magnetosome chains illustrating that magnetite crystals preserved their alignment when the membrane was still present. (D) Purified magnetite aggregating after TES treatment and magnetosome membrane removal. (E) Zoom on a single magnetosome, with the black arrow pointing to the biological membrane surrounding magnetite. (F) Zoom on a magnetite nanocrystal for which the organic membrane has been removed.

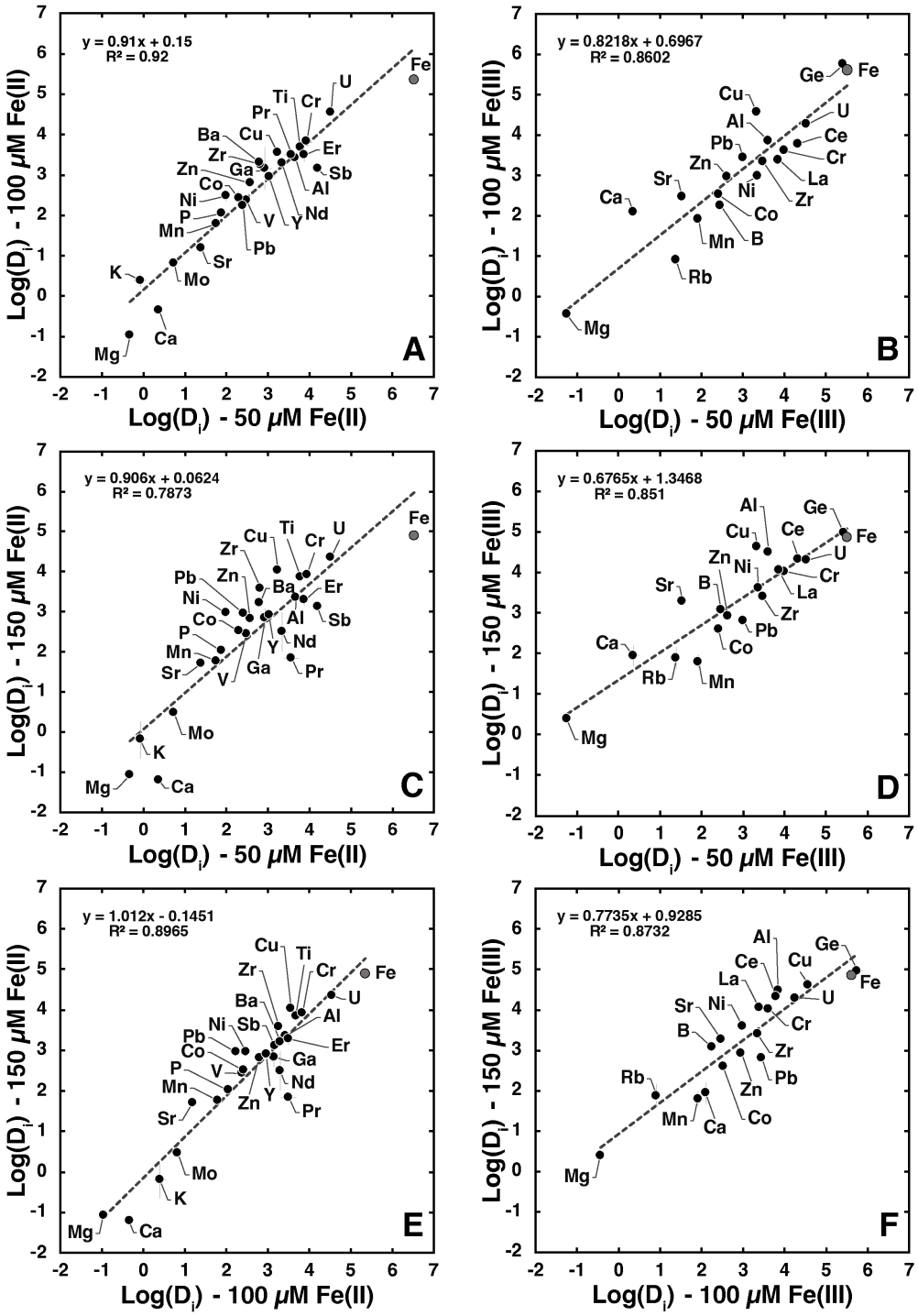

Fig. 2. Comparison of the distribution coefficients (D_i) calculated for every element measured in MV-1 magnetite compared to final growth medium with initial iron concentrations of 50, 100 and 150 µM and (left panels, A, C and E) Fe(II)-ascorbate or (right panels, B, D and F) Fe(III)-citrate as iron source. The decimal logarithms of D_i with a standard deviation lower than 100% are reported in the figures. Regression lines based on least-squares method are indicated for each comparison. Major elements (Mg^{2+}, Ca^{2+}, K^{+}) have extremely low values due to a growth of MV-1 in artificial seawater, highly concentrated in these cations. D_{Fe} (grey dot) is the highest value, sometimes associated with D_{Ge}. This value decreases moderately with the increase of the growth medium iron content.

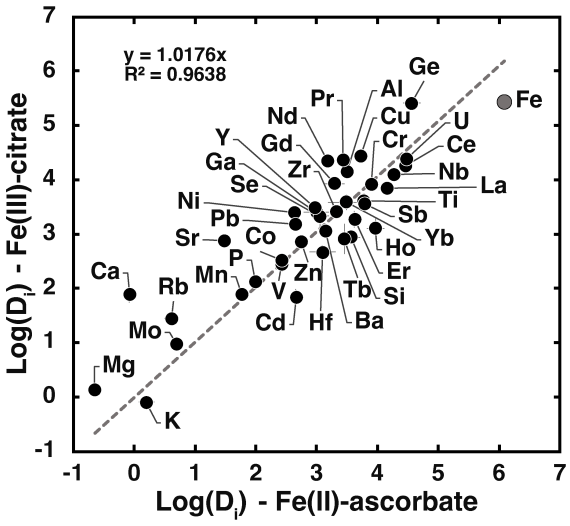

Fig. 3. Average distribution coefficients D_i calculated for MV-1 magnetite in a growth medium containing either Fe(II)-ascorbate or Fe(III)-citrate. Regression line has been obtained with the decimal logarithm of D_i values. D_i estimated for 38 elements are consistent for MV-1 strain, with a maximum discrepancy lower than two orders of magnitude.

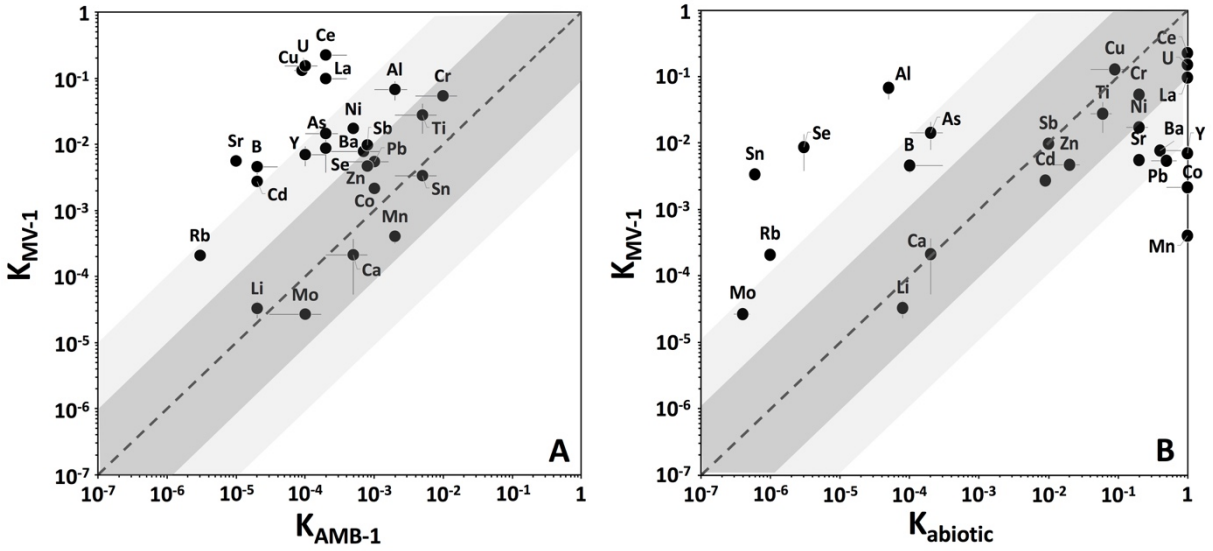

Fig. 4. (A) Average partition coefficients normalized to iron between magnetite produced by MV-1 (this study, K_{MV-1}) and AMB-1 (K_{AMB-1}, data from Amor et al., 2015). It shows that MV-1 accumulates more trace elements in magnetite nanocrystals than AMB-1. (B) Comparison of average values calculated for magnetite produced by MV-1 (K_{MV-1}, this study) and abiotic magnetite ($K_{abiotic}$ data from Amor et al., 2015). $K_i = 1$ indicates that the element i has a similar behavior as iron. In contrast, K_i values lower or higher than 1 imply that the element i is respectively depleted or enriched in magnetite relative to the growth medium or solution from which magnetite precipitates. Dark and light grey zones correspond to areas where $K_{i,Fe}$ calculated for both strains differ within one or two orders of magnitude respectively

(i.e. distance from the 1:1 line, dashed line). The partition coefficients show that MTB magnetite is not as pure as it is usually assumed in the literature (*e.g.* Thomas-Keprta et al., 2000) and contains trace and minor elements in various proportions. Yet, abiotic magnetite is still more enriched in most elements than biosynthesized magnetite, except for Al, As, B, Mo, Rb, Se, and Sn.

Supplementary material

Establishing the content in trace and minor elements of magnetite as a biosignature of magnetotactic bacteria

François P. Mathon, Matthieu Amor, François Guyot, Nicolas Menguy,
Christopher T. Lefevre, Vincent Busigny

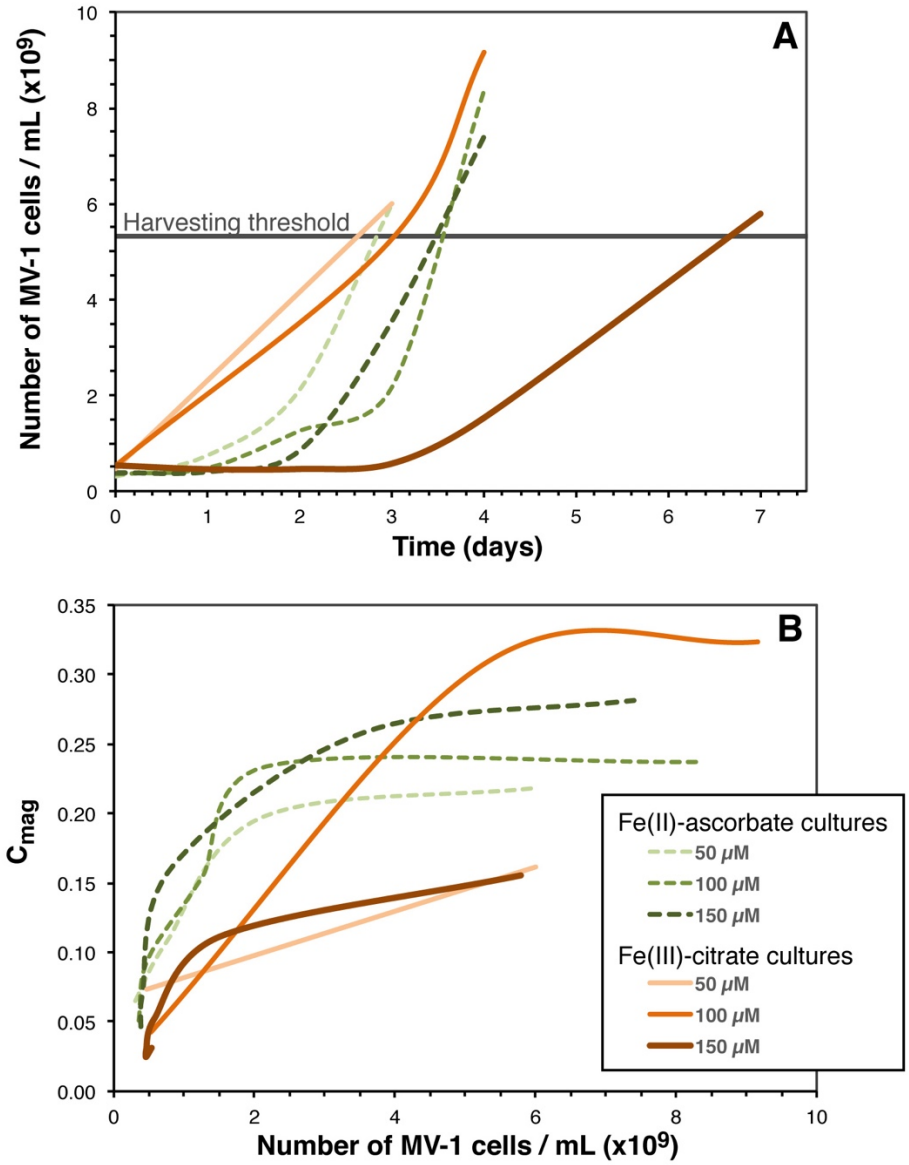

Fig. S1. Monitoring of MV1 cultures for various concentrations of initial Fe(II)-ascorbate (green dotted lines) and Fe(IIII)-citrate (orange lines) conditions. (A) Evolution of the total number of bacteria per milliliter, calculated from OD measurements (OD = 560 nm). (B) Proportion of magnetic cells during bacterial growth (estimated from C_{mag} measurements, see main text for detailed description). When bacterial concentration increases by more than four times relative to initial condition, the proportion of magnetic cells over the whole population becomes relatively stable. In cultures with Fe(II)-ascorbate, the proportion of magnetic cells is correlated with initial iron concentration, suggesting a better efficiency in producing magnetosome at higher Fe concentration.

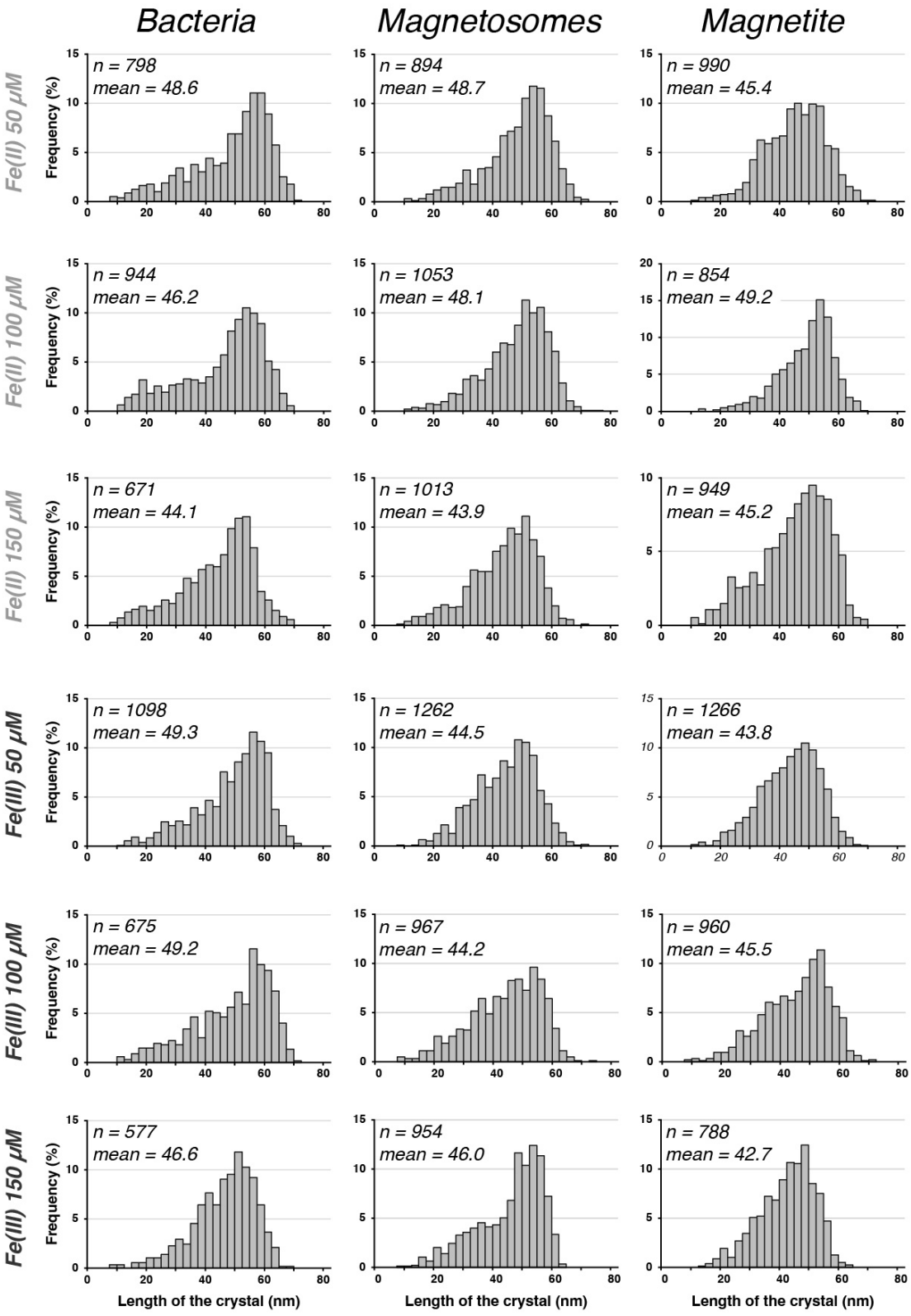

Fig. S2. Size distribution of magnetite nanocrystals produced by MV-1 inside bacterial cells before harvesting, after purification treatment in magnetosome samples, and after detergent treatment to remove membranes of magnetosomes (*i.e.* purified magnetite). The results show identical size distribution at all steps, illustrating a limited bias from analytical treatments.

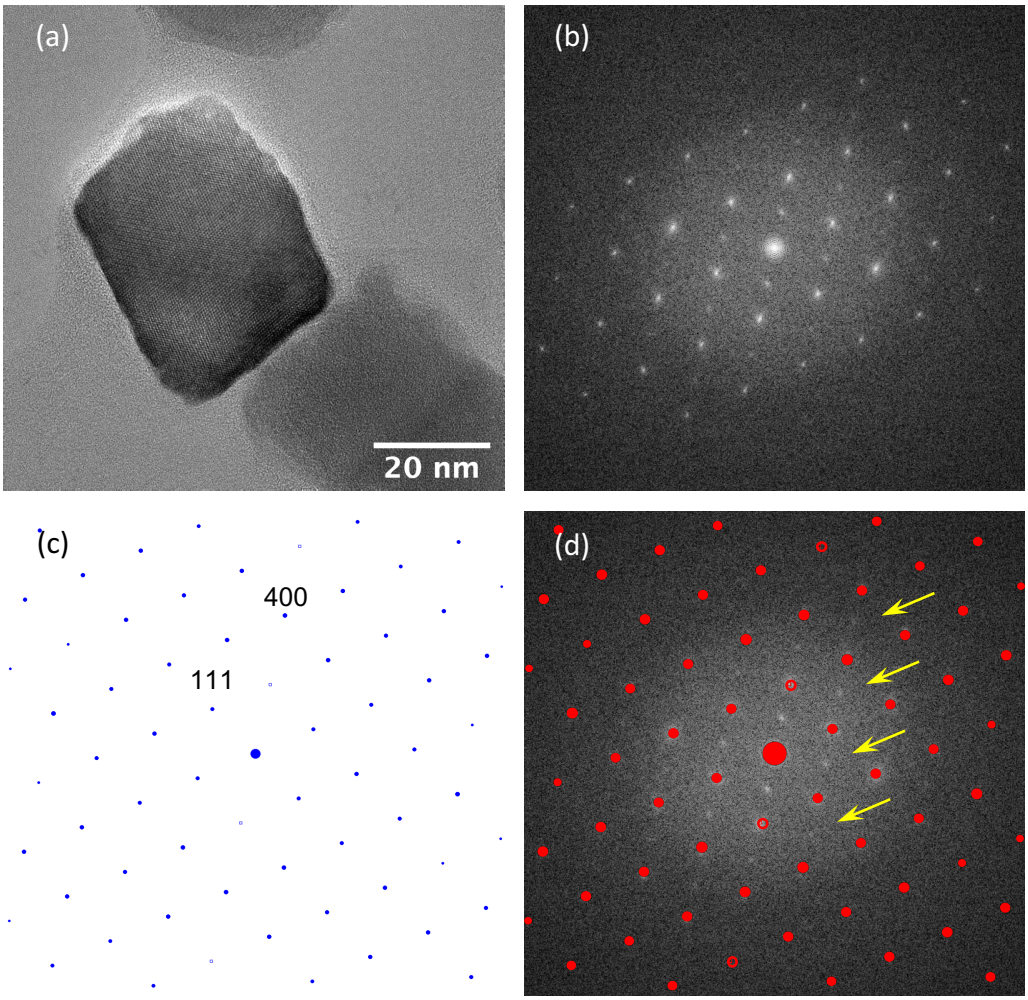

Fig. S3. (a) HR-TEM image of a magnetite nanocrystal produced from MV-1 culture with Fe(II)-ascorbate condition at 50 μM. (b) Fourier transform (FFT) corresponding to the central zone of magnetosome. (c) Simulated diffraction pattern for magnetite along the crystallographic axis <110>. (d) Comparison between FFT-simulation and analyzed pattern showing a few additional points specific to maghemite.

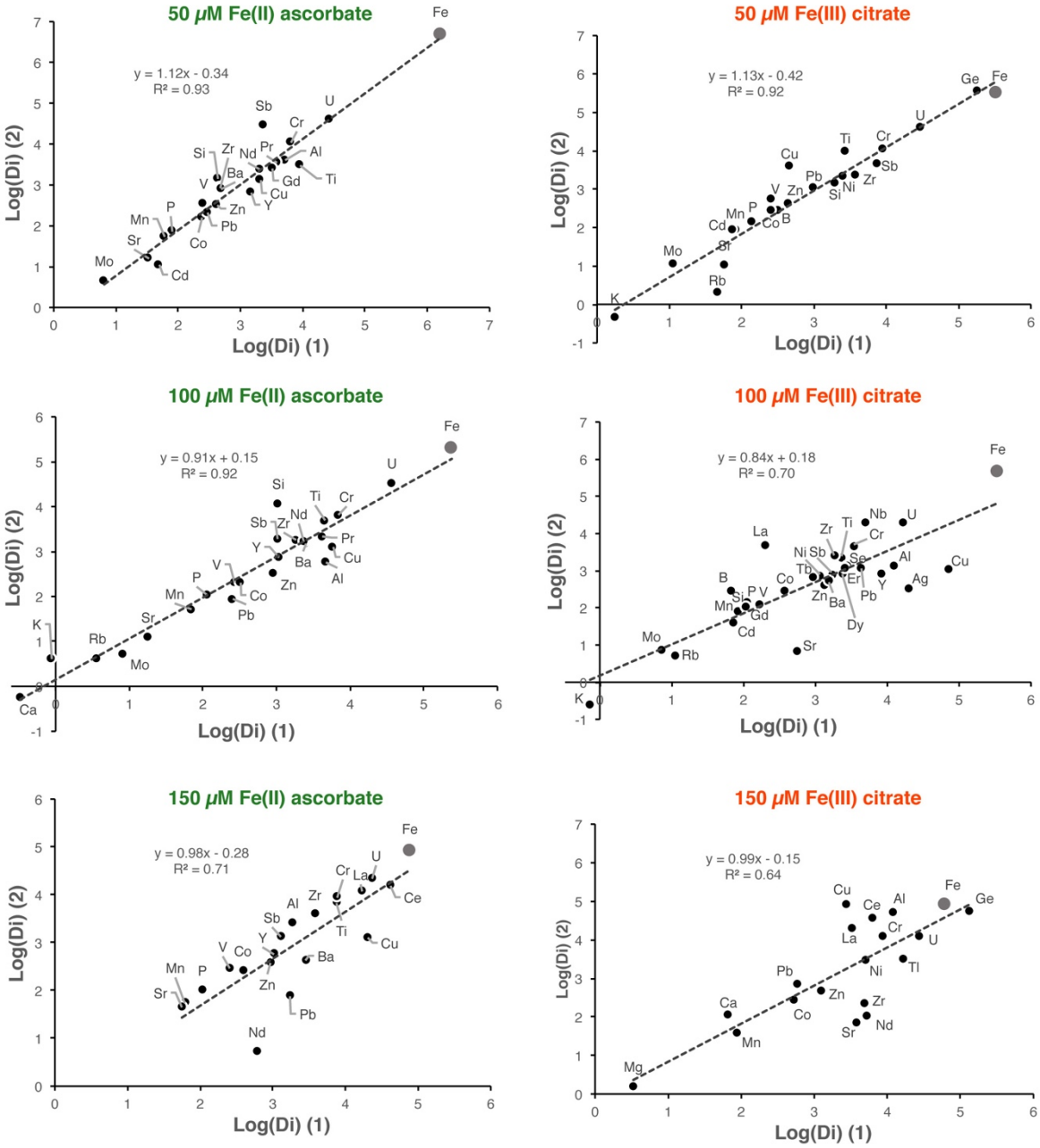

Fig. S4. Comparison of the distribution coefficients (D_i) obtained for replicates (1) and (2) in all culture conditions. Green and orange colors correspond to Fe(II)-ascorbate (left panel) and Fe(III)-citrate (right panel) conditions, respectively. The duplicates show a good correlation with a slope near 1 (dark grey dotted lines and equations on the graph).

Table S1. Growth parameters monitored during Fe(II)-ascorbate and Fe(III)-citrate cultures of MV-1 (cell concentration, pH, Cmag). R#1 to R#10 are individual replicates (1L bottle). Sub-samples were collected once a day for most experiments.

	Day	R#1	R#2	R#3	R#4	R#5	R#6	R#8	R#9	R#10	Average	± 1SD
Fe(II)-ascorbate												
50 uM Fe(II)												
cells/L	0	3,52E+08			2,59E+08			3,06E+08			3,06E+08	4,63E+07
	1	6,45E+08	1,00E+09	7,53E+08	6,30E+08	6,60E+08	8,92E+08	7,69E+08	7,84E+08	5,83E+08	7,46E+08	1,35E+08
	2	1,60E+09	2,94E+09	2,08E+09	1,86E+09	2,02E+09	2,53E+09	2,14E+09	2,11E+09	1,77E+09	2,12E+09	4,05E+08
	3	4,61E+09	7,03E+09	6,22E+09	5,60E+09	6,56E+09	6,71E+09	6,51E+09	5,66E+09	5,00E+09	5,99E+09	8,21E+08
pH	0	6,96	6,97	6,97	6,98	6,95	6,98	6,99	6,95	7,00	6,97	0,02
	1	6,96	6,96	6,97	6,96	6,95	6,96	6,98	6,94	7,00	6,96	0,02
	2	6,95	7,02	7,00	6,97	6,98	7,02	7,00	6,99	7,00	6,99	0,02
	3	7,07	7,05	7,00	6,97	7,02	7,02	7,05	6,99	6,99	7,02	0,03
Cmag	0	0,057			0,078			0,060			0,065	0,011
	1	0,090	0,107	0,104	0,114	0,122	0,105	0,103	0,102	0,118	0,107	0,010
	2	0,179	0,210	0,198	0,202	0,202	0,194	0,210	0,190	0,191	0,197	0,010
	3	0,208	0,211	0,220	0,227	0,216	0,216	0,232	0,213	0,221	0,218	0,008
100 uM Fe(II)												
cells/L	0	3,98E+08	2,90E+08	3,83E+08	3,36E+08	4,14E+08	3,52E+08	4,14E+08	2,28E+08	3,67E+08	3,54E+08	6,15E+07
	1	5,06E+08	4,60E+08	4,91E+08	4,60E+08	5,37E+08	5,99E+08	4,75E+08	5,22E+08	2,90E+08	4,82E+08	8,42E+07
	2	1,26E+09	1,09E+09	1,17E+09	1,14E+09	1,65E+09	1,63E+09	1,32E+09	8,46E+08	1,25E+09	1,26E+09	2,54E+08
	3	1,86E+09	1,93E+09	2,22E+09	2,33E+09	2,20E+09	3,55E+09	2,22E+09	1,37E+09	1,83E+09	2,17E+09	5,95E+08
	4	8,52E+09	8,78E+09	8,62E+09	8,22E+09	9,35E+09	6,60E+09	7,53E+09	8,87E+09	8,76E+09	8,36E+09	8,27E+08
pH	0	7,01	7,00	6,99	6,99	6,98	6,97	6,98	6,99	6,99	6,99	0,01
	1	6,96	6,95	6,95	6,95	6,96	6,96	6,95	6,97	6,96	6,96	0,01
	2	6,89	6,89	6,89	6,88	6,89	6,87	6,90	6,89	6,89	6,89	0,01
	3	6,94	6,92	6,87	6,91	6,90	6,94	6,90	6,89	6,89	6,91	0,02
	4	7,08	7,03	6,97	7,02	7,04	6,97	7,01	7,00	7,03	7,02	0,03
Cmag	0	0,055	0,061	0,056	0,043	0,054	0,057	0,054	0,065	0,014	0,051	0,015
	1	0,088	0,091	0,089	0,091	0,085	0,116	0,090	0,099	0,106	0,095	0,010
	2	0,124	0,161	0,171	0,182	0,110	0,209	0,143	0,157	0,133	0,154	0,031
	3	0,232	0,233	0,246	0,237	0,205	0,271	0,230	0,221	0,229	0,234	0,018
	4	0,229	0,237	0,229	0,240	0,240	0,259	0,234	0,235	0,231	0,237	0,009
150 uM Fe(II)												
cells/L	0	3,98E+08	6,30E+08	3,67E+08	3,98E+08	3,67E+08	3,52E+08	3,06E+08	3,06E+08	3,36E+08	3,84E+08	9,80E+07
	1	2,90E+08	5,52E+08	5,37E+08	3,52E+08	3,83E+08	3,67E+08	3,67E+08	4,44E+08	3,36E+08	4,03E+08	9,00E+07
	2	7,69E+08	7,99E+08	7,53E+08	8,30E+08	9,54E+08	7,99E+08	7,38E+08	1,31E+09	6,76E+08	8,47E+08	1,89E+08
	3	2,61E+09	2,74E+09	2,73E+09	3,73E+09	4,84E+09	3,22E+09	2,70E+09	6,86E+09	2,48E+09	3,55E+09	1,45E+09
	4	6,65E+09	7,61E+09	8,58E+09	7,25E+09	7,00E+09	8,75E+09	6,74E+09	7,19E+09	6,83E+09	7,40E+09	7,74E+08
pH	0	7,07	7,06	7,07	7,09	7,08	7,08	7,07	7,04	7,11	7,07	0,02
	1	6,97	6,97	6,98	6,93	6,95	6,96	6,95	6,95	6,99	6,96	0,02
	2	6,94	6,93	6,97	6,90	6,88	6,89	6,89	6,87	6,94	6,91	0,03
	3	6,94	6,93	6,98	6,95	6,95	6,93	6,94	7,00	6,97	6,95	0,02
	4	7,02	7,00	7,09	7,03	6,97	7,01	7,02	6,97	7,02	7,01	0,04
Cmag	0	0,055	0,034	0,056	0,041	0,042	0,043	0,045	0,045	0,058	0,047	0,008
	1	0,061	0,072	0,073	0,086	0,069	0,056	0,070	0,079	0,058	0,069	0,010
	2	0,134	0,141	0,156	0,178	0,220	0,152	0,116	0,235	0,132	0,163	0,041
	3	0,264	0,213	0,246	0,301	0,302	0,266	0,203	0,293	0,236	0,258	0,037
	4	0,274	0,265	0,267	0,304	0,311	0,279	0,273	0,300	0,259	0,281	0,019

Table S1. Continue.

	Day	R#1	R#2	R#3	R#4	R#5	R#6	R#8	R#9	R#10	Average	± 1SD
Fe(III)-citrate												
50 uM Fe(III)												
cells/L	0	3,67E+08	4,75E+08	3,83E+08	4,60E+08	5,06E+08	3,83E+08	5,22E+08	6,45E+08	4,75E+08	4,68E+08	8,70E+07
	3	6,86E+09	3,52E+09	8,49E+09	4,33E+09	6,20E+09	5,92E+09	7,54E+09	3,92E+09	7,24E+09	6,00E+09	1,74E+09
pH	0	7,01	6,96	7,03	7,00	7,04	7,02	7,01	6,97	7,03	7,01	0,03
	3	6,95	6,90	6,94	6,93	6,97	6,97	7,01	6,94	6,94	6,95	0,03
Cmag	0	0,085	0,077	0,069	0,078	0,075	0,069	0,074	0,056	0,077	0,073	0,008
	3	0,157	0,167	0,146	0,171	0,167	0,160	0,159	0,166	0,161	0,161	0,008
100 uM Fe(III)												
cells/L	0	3,67E+08	5,22E+08	5,37E+08	6,60E+08	6,45E+08	4,29E+08	6,30E+08	5,22E+08	4,44E+08	5,28E+08	1,03E+08
	3	2,77E+09	3,90E+09	7,03E+09	4,58E+09	4,73E+09	4,26E+09	7,90E+09	8,04E+09	4,15E+09	5,26E+09	1,90E+09
	4	7,08E+09	1,05E+10	7,64E+09	9,43E+09	9,23E+09	1,03E+10	7,99E+09	9,06E+09	1,12E+10	9,16E+09	1,39E+09
pH	0	7,01	7,02	6,99	6,99	6,98	7,04	6,99	7,00	7,02	7,00	0,02
	3	6,94	6,97	6,97	6,96	6,96	6,91	6,98	6,97	6,90	6,95	0,03
	4	6,92	6,97	6,94	6,93	6,95	6,99	6,91	6,95	7,00	6,95	0,03
Cmag	0	0,056	0,049	0,037	0,044	0,022	0,040	0,045	0,049	0,039	0,043	0,010
	3	0,317	0,277	0,346	0,343	0,347	0,226	0,349	0,292	0,269	0,307	0,044
	4	0,318	0,278	0,356	0,392	0,389	0,242	0,363	0,292	0,281	0,323	0,054
150 uM Fe(III)												
cells/L	0	5,06E+08	4,75E+08	5,37E+08	5,37E+08	5,37E+08	6,14E+08	4,75E+08	5,99E+08	5,52E+08	5,37E+08	4,82E+07
	1	3,67E+08	3,67E+08	4,91E+08	4,75E+08	4,29E+08	4,91E+08	4,91E+08	5,06E+08	4,91E+08	4,56E+08	5,50E+07
	2	3,52E+08	4,14E+08	4,60E+08	4,75E+08	4,14E+08	5,06E+08	4,75E+08	5,22E+08	5,37E+08	4,62E+08	5,95E+07
	3	3,67E+08	4,91E+08	6,14E+08	6,14E+08	5,52E+08	5,99E+08	5,68E+08	6,60E+08	7,07E+08	5,75E+08	9,95E+07
	4	6,45E+08	1,20E+09	1,83E+09	1,85E+09	1,42E+09	1,42E+09	1,60E+09	1,69E+09	2,11E+09	1,53E+09	4,30E+08
	7	8,33E+09	7,20E+09	4,90E+09	4,15E+09	5,28E+09	3,96E+09	7,44E+09	3,27E+09	7,57E+09	5,79E+09	1,86E+09
pH	0	6,95	6,95	6,91	6,93	6,94	6,93	6,96	6,92	6,96	6,94	0,02
	1	6,98	6,97	6,93	6,95	6,96	6,95	6,96	6,95	6,97	6,96	0,01
	2	6,97	6,95	6,92	6,94	6,95	6,95	6,96	6,95	6,96	6,95	0,01
	3	6,97	6,93	6,90	6,93	6,94	6,93	6,94	6,92	6,92	6,93	0,02
	4	6,93	6,91	6,87	6,91	6,90	6,90	6,89	6,91	6,92	6,90	0,02
	7	6,99	7,00	6,96	6,88	6,93	6,92	6,97	6,90	6,97	6,95	0,04
Cmag	0	0,038	0,026	0,037	0,024	0,037	0,023	0,038	0,035	0,024		0,007
	1	0,028	0,028	0,025	0,026	0,027	0,025	0,013	0,025	0,025	0,025	0,005
	2	0,029	0,027	0,026	0,026	0,041	0,025	0,038	0,025	0,037	0,030	0,006
	3	0,028	0,063	0,057	0,057	0,048	0,047	0,060	0,044	0,065	0,052	0,012
	4	0,090	0,120	0,120	0,132	0,108	0,101	0,113	0,108	0,114	0,112	0,012
	7	0,150	0,154	0,159	0,165	0,154	0,164	0,155	0,154	0,143	0,155	0,007

Table S2. Trace element compositions of magnetite and final growth medium for culture of MV-1 (this study) and AMB-1 and abiotic magnetite (Amor et al., 2015). Concentrations in magnetite correspond to average values measured for all our experiments (this study, Amor et al., 2015). Element concentration in residual solution was calculated from concentration in magnetite and average Di values determined for all experiments.

Element	Concentration in magnetite (ppm)						Concentration in residual solution (ppm)					
	MV-1	± 1SD	AMB-1	± 1SD	Abiotic	± 1SD	MV-1	± 1SD	AMB-1	± 1SD	Abiotic	± 1SD
Ag	1,8E+00	7,2E-01	3,1E+01	4,2E+01	7,8E+01	1,4E+00	2,2E-04	2,5E-06	1,2E-02		7,9E-06	2,5E-06
Al	6,0E+02	2,3E+02	4,8E+01	6,7E+01	2,2E+02	1,3E+01	7,4E-02	4,0E-03	1,5E+00	5,2E-01	1,2E+00	2,7E-02
As	2,2E+00	9,0E-01	1,3E+01	5,9E+00	1,7E+01	8,2E+00	4,7E-04	4,5E-05	7,8E-01	2,1E-01	1,9E-02	3,8E-04
B	1,2E+01	2,3E+00	4,4E+00	4,5E+00	2,4E+02	2,9E+02	3,2E-02	4,5E-04	5,3E+00	5,6E+00	9,8E-01	7,7E-02
Ba	2,8E+00	2,6E-01	1,4E+01	1,6E+01	1,3E+02	7,0E+00	2,5E-03	2,9E-05	5,1E-01	3,1E-01	8,0E-05	5,3E-05
Be							1,8E-04	1,4E-04				
Ca	5,6E+03	3,2E+03	7,1E+01	2,4E+01	2,7E+00	4,2E-02	1,5E+02	1,1E+00	6,3E+00	3,2E+00	4,1E-03	
Cd	3,0E-01	4,0E-02	1,1E+00	5,3E-01	7,0E+01	1,3E+00	1,2E-03	2,6E-05	3,9E-01	4,7E-01	2,1E-03	9,4E-05
Ce	6,9E-01	8,8E-02	5,2E+00	5,2E+00	8,1E+01	3,5E-01	3,0E-05	5,8E-07	4,9E-01	4,5E-01	1,7E-04	2,0E-04
Co	3,5E+01	7,4E-01	5,8E+01	6,5E+01	1,1E+02	1,8E+00	1,3E-01	6,9E-04	1,5E+00	1,2E+00	2,5E-05	1,1E-05
Cr	1,1E+02	2,6E+00	3,3E+02	2,7E+02	1,9E+02	4,8E-01	1,6E-02	7,0E-05	9,4E-01	1,2E-01	2,9E-04	1,9E-05
Cs			1,6E-01	4,3E-03	8,7E+00	1,3E-01	1,0E-04	7,4E-06	7,5E-01	3,2E-01	5,8E-01	6,6E-04
Cu	1,4E+02	4,4E+00	5,9E+00	4,1E+00	1,4E+02	9,9E+00	8,5E-03	2,8E-05	4,4E-01	5,0E-01	4,2E-04	1,8E-04
Dy	1,2E-02	1,0E-02					7,0E-06	3,0E-06				
Er	1,6E-02	1,0E-02					4,5E-06	1,7E-06				
Fe	3,2E+06	1,3E+05					4,5E+00	1,7E-02				
Ga	1,6E-01	1,4E-01	1,9E+01	2,7E+01	3,3E+01	1,5E+00	1,3E-04	3,2E-05	7,4E-01	2,9E-01	3,9E-01	2,8E-04
Gd	1,6E-01	4,9E-02					3,0E-05	8,9E-07				
Ge	1,5E+02	5,0E+02					9,8E-04	2,9E-03				
Hf	3,6E-02	2,5E-02					2,9E-05	1,9E-06				
Ho	6,3E-03	3,1E-03					1,2E-06	2,1E-07				
K	2,1E+02	8,8E+01	3,9E+01	3,4E+01	1,4E+02	5,2E+00	1,9E+02	5,1E+00	1,6E+03	9,3E+02	2,4E+00	1,2E-01
La	2,9E-01	2,8E-02	4,2E+00	5,0E+00	8,3E+01	1,2E+00	2,7E-05	5,9E-07	4,8E-01	4,6E-01	2,1E-05	9,4E-07
Li	1,4E-01	4,0E-02	5,3E-01	3,3E-01	7,2E+01	2,3E+00	8,3E-04	6,1E-05	8,6E-01	4,0E-01	2,3E-01	3,4E-03
Lu	1,8E-03	1,2E-03					6,7E-07	1,7E-07				
Mg	3,4E+02	6,3E+01	1,0E+02	7,2E+01	2,4E+02	7,7E+00	4,4E+02	3,7E+00	5,3E+01	5,4E+01	6,9E-03	
Mn	5,5E+01	7,6E+00	7,6E+02	8,9E+02	1,9E+03	2,6E+01	9,1E-01	5,6E-03	9,3E+00	1,2E+01	4,1E-04	1,9E-05
Mo	5,4E+00	3,4E-01	6,1E+00	1,1E+00	9,6E-01	3,1E-01	9,2E-01	3,7E-03	5,3E+00	6,8E+00	6,6E-01	6,8E-03
Na	6,5E+03	5,5E+03					8,4E+03	6,5E+01				
Nb	5,0E-01	2,7E-01					3,2E-05	1,2E-05				
Nd	1,8E+00	2,1E-01					1,5E-04	1,8E-06				
Ni	1,9E+02	3,6E+02	4,7E+01	2,6E+01	1,3E+02	7,4E-01	1,5E-01	2,8E-01	1,1E+00	2,7E-01	3,0E-04	1,6E-04
P	2,6E+03	3,8E+02					2,6E+01	7,7E-01				
Pb	3,3E+00	9,6E-02	2,8E+01	6,5E+00	7,6E+01	1,3E-01	3,7E-03	1,9E-05	6,2E-01	5,8E-01	3,8E-05	1,2E-05
Pr	5,5E-01	1,5E-01					4,2E-05	4,1E-07				
Rb	1,5E-01	1,8E-02	1,7E-01	3,0E-02	3,4E+00	1,7E-01	1,3E-02	2,2E-05	8,7E-01	8,7E-02	6,8E-01	1,7E-02
Sb	6,3E-01	7,3E-02	1,5E+01	2,0E+01	2,3E+01	5,5E-01	1,6E-04	5,0E-06	6,5E-01	4,5E-01	5,9E-04	6,6E-05
Se	4,0E-01	2,5E-01	9,1E+00	2,4E+00	4,3E+00	7,6E-01	2,5E-04	4,0E-05	5,9E-01	5,7E-01	4,0E-01	4,1E-03
Si	2,3E+03	1,3E+03					1,1E+00	2,1E-01				
Sm	6,7E-02	5,9E-02					1,0E-05	4,0E-06				
Sn	3,2E-02	3,0E-03	1,1E+02	5,3E+01	4,2E-01	0,0E+00	1,1E-04	4,5E-06	5,5E-01	2,7E-01	1,8E-01	7,3E-03
Sr	8,6E+00	1,5E-01	4,3E-01	2,1E-02	1,5E+02	2,1E+00	2,2E-02	1,0E-04	5,4E-01	9,3E-02	2,6E-04	9,4E-06
Tb	2,2E-03	1,0E-03					1,2E-06	1,4E-07				
Th	7,2E-01	1,6E+00	3,3E+01	4,6E+01	8,4E+01	7,2E-01	4,0E-05	8,1E-05	3,5E-01	4,4E-01	1,0E-05	3,5E-06
Ti	2,6E+01	1,6E+01	1,1E+02	1,2E+02	7,5E+01	1,4E+01	5,1E-03	1,1E-03	5,3E-01	9,1E-02	4,1E-04	2,7E-04
Tl	2,3E-01	6,2E-02	4,5E+00	5,3E+00	7,2E+01	1,8E+00	2,4E-05	1,1E-06	5,9E-01	2,3E-01	1,5E-04	3,5E-05
U	5,5E-01	5,6E-02	1,5E+01	2,1E+01	8,5E+01	6,5E-01	2,2E-05	8,3E-07	5,1E-01	2,6E-01	1,7E-03	2,8E-04
V	5,2E-01	1,7E-01	1,7E+00		4,2E+01	5,5E+00	2,0E-03	3,4E-05	5,1E-01	1,7E-02	4,6E-03	9,4E-05
Y	4,5E-02	1,2E-02	2,1E+00	2,7E+00	8,7E+01	2,0E+00	1,6E-05	2,3E-06	5,4E-01	4,7E-01	2,5E-05	0,0E+00
Yb	1,0E-02	1,7E-02					2,9E-06	2,9E-06				
Zn	1,4E+02	3,3E+00	6,2E+01	2,3E+01	1,4E+02	1,8E+01	2,3E-01	9,9E-04	1,5E+00	4,8E-02	5,2E-03	5,7E-03
Zr	2,5E+00	2,1E-01					1,2E-03	7,4E-06				

Table S3. Average distribution coefficients (Di) between magnetite and final growth medium for culture of MV-1. The cultures were performed under various Fe sources (Fe(II)-ascorbate and Fe(III)-citrate) at initial concentrations of 50, 100 and 150 uM.

Element	Fe(III)-citrate						Fe(II)-ascorbate					
	50 µM		100 µM		150 µM		50 µM		100 µM		150 µM	
	Average	± 1SD	Average	± 1SD	Average	± 1SD	Average	± 1SD	Average	± 1SD	Average	± 1SD
Li							1,62E+02	1,09E+02				
B	2,94E+02	3,07E+01	1,76E+02	1,25E+01	1,22E+03	2,01E+02						
Na	2,23E-01	8,94E-02	1,80E-01	6,63E-03	6,08E+00	4,92E+00	2,83E-01	1,22E-02	2,35E-01	1,85E-02	6,28E-02	1,61E-02
Mg	5,73E-02	4,42E-03	3,61E-01	9,66E-03	2,46E+00	3,81E-01	4,78E-01	1,93E-02	1,08E-01	2,77E-02	8,45E-02	2,11E-03
Al	4,19E+03	1,80E+02	7,02E+03	8,45E+02	3,14E+04	1,12E+04	4,62E+03	1,24E+03	2,63E+03	4,59E+02	2,23E+03	1,55E+02
Si	1,68E+03	1,93E+02	8,31E+01	2,04E+01			9,23E+02	2,24E+02	6,35E+03	2,57E+03		
P	1,39E+02	1,47E+01	1,28E+02	1,23E+01			7,59E+01	5,43E+00	1,11E+02	1,08E+01	1,04E+02	9,98E+00
K	1,10E+00	3,43E-01	4,88E-01	1,07E-01			8,38E-01	2,77E-01	2,47E+00	9,48E-01	6,39E-01	5,02E-01
Ca	2,28E+00	6,35E-01	1,25E+02	2,73E+00	8,85E+01	6,33E+01	2,38E+00	1,40E-01	4,59E-01	6,80E-02	6,07E-02	3,44E-03
Ti	5,92E+03	2,72E+03	2,29E+03	1,27E+03			6,04E+03	1,95E+03	4,76E+03	8,16E+02	7,11E+03	2,60E+03
V	4,02E+02	1,82E+02	1,46E+02	3,09E+01			3,05E+02	4,84E+01	2,36E+02	1,74E+01	2,73E+02	4,38E+01
Cr	9,97E+03	2,07E+02	4,09E+03	4,81E+01	1,07E+04	8,74E+01	8,65E+03	2,65E+02	6,73E+03	8,71E+01	8,20E+03	1,33E+02
Mn	8,49E+01	2,91E+00	8,16E+01	1,96E+00	6,33E+01	3,24E+01	5,70E+01	1,74E+00	6,10E+01	2,01E+00	5,79E+01	1,15E+00
Fe	3,25E+05	3,07E+03	4,13E+05	3,62E+03	7,27E+04	7,43E+02	3,36E+06	1,47E+05	2,22E+05	5,50E+03	8,01E+04	3,44E+02
Co	2,61E+02	5,25E+00	3,33E+02	4,05E+00	3,97E+02	2,28E+00	2,00E+02	6,38E+00	2,64E+02	5,94E+00	3,22E+02	2,37E+00
Ni	2,34E+03	9,02E+01	9,46E+02	2,47E+01	4,13E+03	6,43E+01	9,74E+01	7,11E+00	2,99E+02	8,81E+01	9,10E+02	2,26E+02
Cu	2,18E+03	5,45E+01	3,69E+04	6,66E+02	4,27E+04	1,36E+03	1,72E+03	5,12E+01	3,58E+03	1,24E+02	1,08E+04	8,31E+01
Zn	4,29E+02	1,74E+01	9,03E+02	9,99E+00	8,64E+02	8,40E+00	3,71E+02	1,04E+01	6,28E+02	1,80E+01	6,52E+02	7,60E+00
Ga	3,50E+03	1,32E+03	1,37E+03	1,11E+03			8,54E+02	2,96E+02	1,43E+03	1,20E+03	6,81E+02	3,49E+02
Ge	2,68E+05	6,33E+04	5,62E+05	1,77E+05	9,52E+04	2,13E+04					3,66E+04	1,21E+04
As							3,63E+03	8,50E+02	5,73E+03	2,08E+03		
Se			2,11E+03	1,14E+03							1,13E+03	3,67E+02
Rb	2,46E+01	3,63E+00	8,17E+00	6,28E-01	7,70E+01	4,33E+01	4,26E+00	2,06E+00	3,96E+00	1,51E+00		
Sr	3,46E+01	1,81E+00	2,89E+02	3,84E+00	1,94E+03	1,56E+01	2,48E+01	1,29E+00	1,53E+01	4,62E-01	5,03E+01	3,34E+00
Y	2,79E+01	2,61E+01	4,63E+03	3,78E+02			1,07E+03	3,98E+02	9,08E+02	3,71E+02	8,03E+02	2,93E+02
Zr	3,04E+03	4,12E+02	2,21E+03	9,59E+01	2,54E+03	7,54E+01	6,54E+02	1,00E+02	1,83E+03	1,30E+02	3,81E+03	2,16E+02
Nb			1,26E+04	3,11E+03			2,67E+04	2,75E+03	1,02E+04	6,87E+02		
Mo	1,11E+01	4,54E-01	7,33E+00	1,99E-01			5,48E+00	2,54E-01	6,66E+00	2,18E-01	2,90E+00	6,39E-01
Ag			1,03E+04	3,18E+03								
Cd	7,85E+01	6,24E+01	5,63E+01	1,82E+01			3,05E+01	1,36E+01			1,32E+03	3,11E+01
Sn											2,78E+02	1,50E+01
Sb	5,99E+03	7,53E+02	1,26E+03	2,00E+02			1,57E+04	8,16E+02	1,47E+03	1,49E+02	1,31E+03	2,10E+02
Cs												
Ba	1,19E+03	1,71E+02	1,08E+03	6,49E+01			6,37E+02	7,65E+01	2,01E+03	1,28E+02	1,62E+03	1,27E+02
La	7,32E+03	5,11E+02	2,41E+03	8,75E+01	1,14E+04	3,81E+02					1,44E+04	1,28E+03
Ce	2,17E+04	4,14E+03	6,10E+03	2,11E+02	2,17E+04	7,83E+02					2,86E+04	3,56E+03
Pr	6,56E+04	1,75E+04	5,98E+01	1,25E+01	2,88E+03	1,19E+03	3,68E+03	1,60E+03	3,17E+03	5,23E+02	6,89E+01	3,08E+00
Nd	8,51E+04	7,24E+03	7,61E+01	1,47E+01	2,70E+03	3,71E+02	2,21E+03	6,25E+02	2,00E+03	5,71E+02	3,06E+02	2,49E+02
Sm							9,24E+03	5,27E+03	3,72E+03	1,06E+03		
Gd	3,18E+04	7,33E+03	1,08E+02	5,26E+01			2,88E+03	1,31E+03			1,11E+02	2,52E+01
Tb			8,23E+02	6,10E+02			3,75E+03	1,02E+03	1,92E+03	4,36E+02		
Dy			1,65E+03	7,71E+02								
Ho	1,07E+03	1,00E+03	1,48E+03	4,32E+02			9,25E+03	2,96E+03				
Er			1,87E+03	7,45E+02			7,57E+03	1,58E+03	3,13E+03	1,16E+03	1,91E+03	5,69E+02
Yb									1,62E+03	1,46E+03		
Lu									2,68E+03	1,03E+03		
Hf	4,61E+02	1,36E+02							9,47E+02	4,89E+02	1,97E+03	1,60E+03
Tl					9,89E+03	2,19E+03						
Pb	1,02E+03	5,02E+01	2,80E+03	5,60E+01	6,53E+02	8,43E+00	2,54E+02	9,08E+00	1,71E+02	4,65E+00	9,00E+02	9,18E+00
Th					1,78E+04	4,69E+03						
U	3,45E+04	1,26E+03	1,83E+04	9,90E+02	2,02E+04	1,87E+03	3,29E+04	1,99E+03	3,51E+04	2,02E+03	2,26E+04	1,63E+03